



# Degradation of the antibiotic trimethoprim by electrochemical advanced oxidation processes using a carbon-PTFE air-diffusion cathode and a boron-doped diamond or platinum anode

Francisca C. Moreira<sup>a</sup>, Sergi Garcia-Segura<sup>b</sup>, Rui A.R. Boaventura<sup>a</sup>,  
Enric Brillas<sup>b,\*\*</sup>, Vítor J.P. Vilar<sup>a,\*</sup>

<sup>a</sup> LSRE – Laboratory of Separation and Reaction Engineering – Associate Laboratory LSRE/LCM, Departamento de Engenharia Química, Faculdade de Engenharia, Universidade do Porto, Rua Dr. Roberto Frias, 4200-465 Porto, Portugal

<sup>b</sup> Laboratori d'Electroquímica dels Materials i del Medi Ambient, Departament de Química Física, Facultat de Química, Universitat de Barcelona, Martí i Franquès 1-11, 08028 Barcelona, Spain

## ARTICLE INFO

### Article history:

Received 25 March 2014

Received in revised form 26 May 2014

Accepted 29 May 2014

Available online 6 June 2014

### Keywords:

Trimethoprim

EAOPs

Photoelectro-Fenton

Oxidation products

Real wastewater

## ABSTRACT

The degradation of 20.0 mg L<sup>-1</sup> of trimethoprim (TMP), an antibiotic commonly detected in wastewaters, in an aqueous solution with 7.0 g L<sup>-1</sup> Na<sub>2</sub>SO<sub>4</sub> was accomplished by electrochemical advanced oxidation processes (EAOPs) such as anodic oxidation with electrogenerated H<sub>2</sub>O<sub>2</sub> (AO-H<sub>2</sub>O<sub>2</sub>), electro-Fenton (EF), photoelectro-Fenton (PEF) and solar photoelectro-Fenton (SPEF), as well as by the classical Fenton and photo-Fenton processes. All experiments were performed in a novel 2.2 L lab-scale flow plant equipped with compound parabolic collectors (CPCs) and an electrochemical filter-press cell with a BDD or Pt anode and a carbon-PTFE air-diffusion cathode to electrogenerate H<sub>2</sub>O<sub>2</sub>. The effect of initial Fe<sup>2+</sup> concentration, current density and pH on the PEF method with the BDD anode (PEF-BDD) was firstly assessed by means of TMP and dissolved organic carbon (DOC) decays, aiming to establish a treatment process using minimal iron concentration, adequate current density/H<sub>2</sub>O<sub>2</sub> production and maximal pH. This treatment was efficiently performed using a low Fe<sup>2+</sup> dose of 2.0 mg L<sup>-1</sup>, a low current density of 5 mA cm<sup>-2</sup> and pH of 3.5 without iron precipitation. The relative oxidation ability of EAOPs using the BDD/air-diffusion cell increased in the order: AO-H<sub>2</sub>O<sub>2</sub> < EF < PEF < SPEF. The EF-BDD and PEF-BDD processes were more effective than the comparable Fenton and photo-Fenton ones. The PEF-BDD process exhibited slightly faster TMP degradation than the PEF-Pt one, whereas in SPEF the influence of the anode was almost negligible. After ca. 37 kJ L<sup>-1</sup> UV energy, 77 and 73% mineralization with 30 and 26% current efficiency and 1.2 and 0.9 kWh m<sup>-3</sup> energy cost were obtained, respectively. It was found a slow and partial TMP mineralization mainly linked to the formation of a high content of hardly oxidizable N-derivatives, containing the major part of N. Up to 18 aromatic products and 19 hydroxylated derivatives were detected by LC-MS during TMP degradation by PEF-Pt. An additional SPEF-Pt experiment using a real wastewater matrix spiked with TMP attained slower TMP and DOC decays.

© 2014 Elsevier B.V. All rights reserved.

## 1. Introduction

Pharmaceuticals such as antibiotics, antipyretics, analgesics and hormones, and their bioactive metabolites are continuously introduced into the aquatic systems, where they are detected at trace concentrations (ng L<sup>-1</sup> or µg L<sup>-1</sup> levels) [1,2]. The presence of these compounds constitutes a serious environmental problem

since they are resistant to biological degradation processes, escaping almost intact from conventional wastewater treatment plants (WWTPs), and, in addition, they are toxic and cause other negative effects to humans and other living organisms as they are intended to have physiological effect at trace concentrations [3–5]. Among pharmaceuticals, antibiotics have been recently classified as a priority risk group since they may cause resistance in bacterial populations, making them, in a near future, ineffective in the treatment of several diseases [6]. Trimethoprim (TMP) is an antibiotic commonly prescribed alone or in combination with a sulfonamide (e.g., sulfamethoxazole, sulfadiazine or sulfamoxole) for the treatment of specific bacterial infections, including gastro,

\* Corresponding author. Tel.: +351 918257824; fax: +351 225081674.

\*\* Corresponding author. Tel.: +34 934021223; fax: +34 934021231.

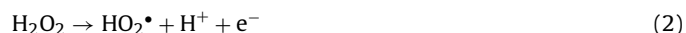
E-mail addresses: [brillas@ub.edu](mailto:brillas@ub.edu) (E. Brillas), [vilar@fe.up.pt](mailto:vilar@fe.up.pt) (V.J.P. Vilar).

respiratory and urinary infections in both human and veterinary medicine [7]. TMP has been detected in surface waters, WWTPs influents and effluents and hospital effluents at concentrations of 0.003–4.30  $\mu\text{g L}^{-1}$  [8,9]. Since TMP cannot be degraded by conventional treatments, a promising approach to the remediation of wastewaters contaminated with high contents of this antibiotic is the application of innovative advanced oxidation processes (AOPs) and electrochemical AOPs (EAOPs), alone or in combination with technologies like nanofiltration and reverse osmosis to concentrate the pollutant before its treatment [10,11].

AOPs comprise a large variety of methods involving (i) ozone and ozone based processes ( $\text{O}_3$ ,  $\text{O}_3/\text{UV}$ ,  $\text{O}_3/\text{H}_2\text{O}_2$ ), (ii) hydrogen peroxide ( $\text{H}_2\text{O}_2$ ) combined with UV radiation ( $\text{H}_2\text{O}_2/\text{UV}$ ), (iii) photocatalysis with titanium dioxide ( $\text{TiO}_2/\text{UV}$ ) and combined with  $\text{H}_2\text{O}_2$  ( $\text{TiO}_2/\text{UV}/\text{H}_2\text{O}_2$ ) and (iv) Fenton's reaction based processes (Fenton –  $\text{Fe}^{2+}/\text{H}_2\text{O}_2$ , photo-Fenton –  $\text{Fe}^{2+}/\text{H}_2\text{O}_2/\text{UV}$  and solar photo-Fenton –  $\text{Fe}^{2+}/\text{H}_2\text{O}_2/\text{UV-vis}$ ). They are characterized by the production of extremely reactive and unselective hydroxyl radical ( $\bullet\text{OH}$ ), which is able to oxidize and mineralize almost all organic compounds to  $\text{CO}_2$ , water and inorganic ions [12]. One of the main drawbacks of these processes is the high cost associated with reagents consumption, specifically high consumption of  $\text{H}_2\text{O}_2$ , which can be surpassed by the application of EAOPs where  $\text{H}_2\text{O}_2$  is directly electrogenerated at the cathode of the cell from the two-electron reduction of injected  $\text{O}_2$  (Eq. (1)), usually at carbon felts [13,14] and carbon-polytetrafluoroethylene (PTFE) gas ( $\text{O}_2$  or air) diffusion electrodes [15,16].

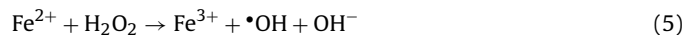


The simplest EAOP based on the cathodic generation of  $\text{H}_2\text{O}_2$  is the anodic oxidation with electrogenerated  $\text{H}_2\text{O}_2$  (AO- $\text{H}_2\text{O}_2$ ), where organic pollutants are oxidized by (i) weak oxidizing agents as  $\text{H}_2\text{O}_2$  formed from Eq. (1) and hydroperoxyl radicals ( $\text{HO}_2\bullet$ ) produced from  $\text{H}_2\text{O}_2$  oxidation to  $\text{O}_2$  at the anode (Eqs. (2) and (3)), (ii) direct electron transfer to the anode M and/or (iii) adsorbed  $\bullet\text{OH}$ , denoted as  $\text{M}(\bullet\text{OH})$ , formed as intermediate of  $\text{O}_2$  evolution from water oxidation at the anode surface (Eq. (4)) [17].

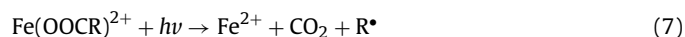


Boron-doped diamond (BDD) thin-film electrodes are usually preferred for water remediation since they produce very high amounts of weakly physisorbed hydroxyl radical (BDD( $\bullet\text{OH}$ )) from Eq. (4), which results in a much greater  $\text{O}_2$ -overpotential of BDD anode in comparison with other materials like Pt and consequently in the enhancement of organics removal [16,18–20].

The addition of low amounts of  $\text{Fe}^{2+}$  ion as catalyst to react with electrogenerated  $\text{H}_2\text{O}_2$  producing  $\text{Fe}^{3+}$  and  $\bullet\text{OH}$  from Fenton's reaction (5) results in the simplest EAOP based on this reaction, the electro-Fenton (EF) method [21].



This process can be improved by the irradiation of the contaminated solution with UVA light, originating the UVA photoelectro-Fenton (PEF) process, where the pollutant degradation is accelerated by (i) the photoreduction of photoactive  $\text{Fe(III)-hydroxy}$  complexes like  $\text{FeOH}^{2+}$ , the most photoactive  $\text{Fe(III)-hydroxy}$  complex, regenerating more  $\text{Fe}^{2+}$  and producing more  $\bullet\text{OH}$ , as shown in Eq. (6) [22], and (ii) the direct photolysis of complexes formed between  $\text{Fe}^{3+}$  and some organic intermediates, especially those containing the carboxylate group according to the general Eq. (7), also regenerating  $\text{Fe}^{2+}$  ion [23–25].



A clear disadvantage of the PEF system is the high cost arising from the use of UVA lamps and, as a result, a process using sunlight ( $\lambda > 300\text{ nm}$ ) as a renewable and inexpensive energy source, the called solar PEF (SPEF), is a much more appealing alternative [26]. In contrast with the classical chemical methods based on Fenton's reaction, in the EF, PEF and SPEF processes the  $\text{Fe}^{2+}$  ion is continuously regenerated by the cathodic reduction of  $\text{Fe}^{3+}$  (Eq. (8)), thus enhancing the Fenton's reaction (5) and thus higher amounts of  $\bullet\text{OH}$  are produced [27].



While AOPs like ozonation [10,28], photocatalysis with  $\text{TiO}_2$  and in combination with  $\text{H}_2\text{O}_2$  [29–31] and photo-Fenton [31,32], being the two latter performed under artificial and natural solar radiation, have been applied to degrade TMP, less is known over the use of EAOPs since only one paper has been published dealing with the AO treatment using a BDD anode [33]. Therefore, one can infer the importance of checking the viability of more powerful methods such as AO- $\text{H}_2\text{O}_2$ , EF, PEF and SPEF to remove TMP and its by-products from synthetic wastewaters.

The present paper reports a comparative study on the degradation of 20.0  $\text{mg L}^{-1}$  TMP aqueous solutions with 7.0  $\text{g L}^{-1}$   $\text{Na}_2\text{SO}_4$  by AO- $\text{H}_2\text{O}_2$ , EF, PEF and SPEF methods for wastewater treatment. Classical Fenton and photo-Fenton processes were also comparatively examined. All the treatments were evaluated in terms of TMP and dissolved organic carbon (DOC) concentration decays. They were performed in a novel 2.2 L lab-scale flow plant containing compound parabolic collectors (CPCs) and an electrochemical cell composed of a BDD or Pt anode and a carbon-PTFE air-diffusion cathode. This system was characterized from the photonic flux reaching the solution in PEF experiments by actinometry and  $\text{H}_2\text{O}_2$  accumulation in function of current density ( $j$ ). The influence of initial  $\text{Fe}^{2+}$  concentration,  $j$  and pH on the PEF process was assessed in a first approach, targeting to establish a treatment process using minimal  $\text{Fe}^{2+}$  concentration (below the Portuguese discharge limit), adequate current density/ $\text{H}_2\text{O}_2$  production and maximal pH. The effect of BDD and Pt anodes under PEF and SPEF conditions was examined. Generated short-chain carboxylic acids and inorganic ions were followed by different techniques and aromatic products were detected by liquid chromatography-mass spectrometry (LC-MS). The degradation of 20.0  $\text{mg L}^{-1}$  TMP spiked in a real wastewater matrix was also assessed using the SPEF-Pt system.

## 2. Experimental

### 2.1. Chemicals

Trimethoprim ( $\text{C}_{14}\text{H}_{18}\text{N}_4\text{O}_3$ ,  $\geq 99.0\%$ ) was of HPLC grade purchased from Sigma-Aldrich. Sodium sulfate anhydrous, used as background electrolyte, and iron(II) sulfate heptahydrate, used as catalyst, were of analytical grade purchased from Merck and Panreac, respectively. Concentrated sulfuric acid and sodium hydroxide, both of analytical grade and used for pH adjustment, were supplied by Pronalab and Merck, respectively. Hydrogen peroxide ( $>30\%$ , w/v) was of analytical grade purchased from Fisher Chemical. All the other chemicals were either of HPLC grade or analytical grade supplied by VWR-Prolabo, Sigma-Aldrich, Panreac, Merck, Fisher Chemical, Pronalab and Alfa Aesar. All the solutions were prepared with ultrapure water produced by a Millipore® Direct-Q system (18.2  $\text{M}\Omega\text{ cm}$  resistivity at 25 °C).

## 2.2. Real wastewater matrix

A real wastewater sample was collected after secondary treatment in an urban WWTP of Northern Portugal. The physicochemical characterization of the effluent is presented in Table SM-1. A 20.0 mg L<sup>-1</sup> TMP spiked effluent was submitted to treatment.

## 2.3. Experimental set-up

Electrochemical tests were carried out in a lab-scale flow plant with 2.2 L of total capacity. A sketch of this novel plant is shown in Fig. 1a. Its main components are: (i) a 1.5 L cylindrical glass vessel as reservoir thermostated at 20 °C, (ii) a photoreactor with CPCs of 694 mL irradiated volume and (iii) an electrochemical filter-press MicroFlowCell reactor, schematized in Fig. 1b, with a 10 cm<sup>2</sup> BDD or Pt anode and a 10 cm<sup>2</sup> carbon-PTFE air-diffusion cathode. A detailed description of the characteristics of these components and the

system operation during the different electrochemical and chemical trials are given in Supplementary Material.

In the PEF tests, the irradiation was provided by a Philips TL 6W/08 fluorescent blacklight blue lamp, which emits UVA light in the wavelength region between 350 and 410 nm with  $\lambda_{\text{max}}$  at 360 nm (see Fig. 2). In the SPEF trials, the photoreactor was tilted 41° (local latitude) and the solar radiation was measured by the global UV radiometer placed at the same angle, which provides the incident energy in W m<sup>-2</sup> from 280 to 400 nm. The accumulated UV energy ( $Q_{UV,n}$ , in kJ L<sup>-1</sup>) received on any surface with regard to the sun in a time interval  $\Delta t$  per unit of volume of water inside the reactor was calculated as follows [34]:

$$Q_{UV,n} = Q_{UV,n-1} + \Delta t_n \overline{UV}_{G,n} \frac{A_r}{1000 \times V_t}; \quad \Delta t_n = t_n - t_{n-1} \quad (9)$$

where  $t_n$  is the time corresponding to the  $n$ -water sample (s),  $V_t$  is the total volume of solution (L),  $A_r$  is the illuminated collector

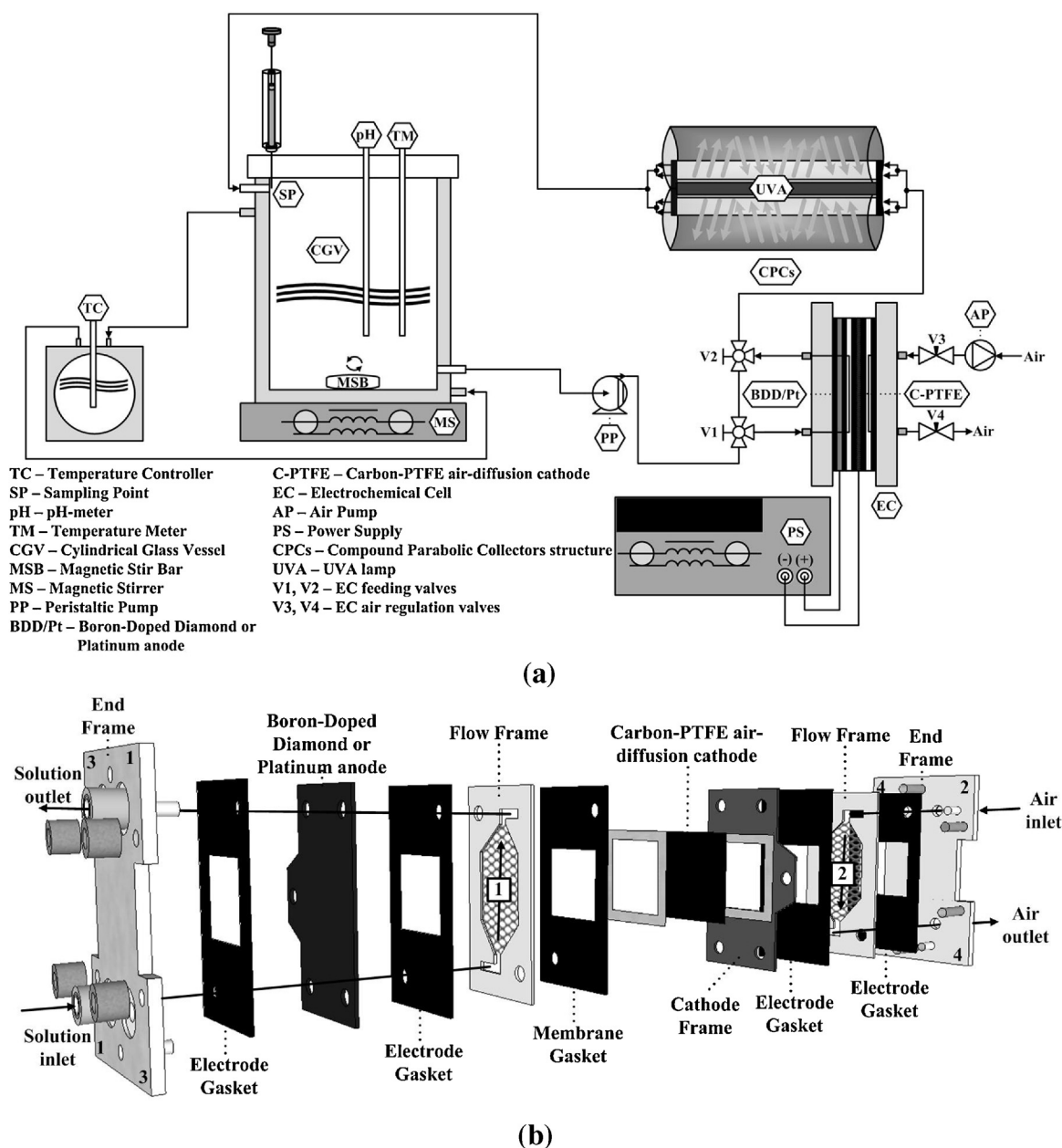
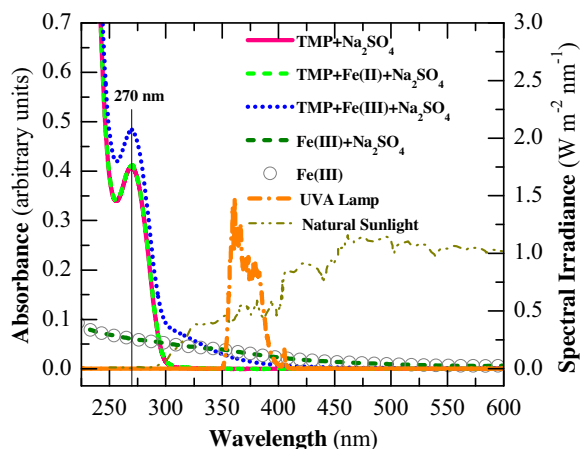


Fig. 1. Sketches of (a) the experimental set-up of the lab-scale flow plant and (b) the one-compartment filter-press MicroFlowCell reactor.



**Fig. 2.** Absorption spectra of different solutions at pH = 3.5, [TMP] = 20.0 mg L<sup>-1</sup>, [Na<sub>2</sub>SO<sub>4</sub>] = 7.0 g L<sup>-1</sup>, [Fe<sup>2+</sup>] = 2.0 mg L<sup>-1</sup> and [Fe<sup>3+</sup>] = 2.0 mg L<sup>-1</sup>. The spectral irradiance of the UVA lamp and natural sunlight are also shown.

surface area (0.041 m<sup>2</sup>) and  $\overline{UV}_{G,n}$  is the average solar ultraviolet radiation (W m<sup>-2</sup>) measured during the period  $\Delta t_n$  (s).

#### 2.4. Actinometric experiments

The following actinometric measurements were performed to determine the photonic flux entering the system in PEF experiments when using the UVA lamp: (i) ferrioxalate actinometry using either crystals of K<sub>3</sub>[Fe(C<sub>2</sub>O<sub>4</sub>)<sub>3</sub>]·3H<sub>2</sub>O or [Fe(C<sub>2</sub>O<sub>4</sub>)<sub>3</sub>]<sup>3-</sup> ion prepared in situ and (ii) 2-nitrobenzaldehyde (2-NB) actinometry. The chemicals, experimental procedures, calculations and analytical determinations used in these tests are described in Supplementary Material.

#### 2.5. Analytical determinations

Before analysis, all the samples were filtered by 0.45 μm Nylon filters from Whatman. The analytical procedures for TMP concentration measurement and detection of generated carboxylic acids, inorganic ions and aromatic products are reported in Supplementary Material. Before TMP analysis, 1 M methanol, a well-known •OH scavenger ( $k_{OH} = 9.7 \times 10^8$  M<sup>-1</sup> s<sup>-1</sup>) [35], was added to the samples in order to stop the mineralization process. The energy consumption per unit TMP mass (EC<sub>TMP</sub>, in kWh kg TMP<sup>-1</sup>) was obtained from the TMP concentration decay according to Eq. (10) [26]:

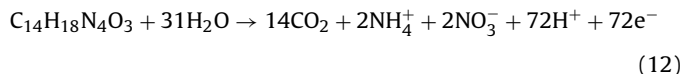
$$EC_{TMP} = \frac{1000E_{cell}It}{V_s \Delta(TMP)_{exp}} \quad (10)$$

where 1000 is a conversion factor (mg g<sup>-1</sup>),  $E_{cell}$  is the average applied cell voltage (V),  $I$  is the applied current (A),  $t$  is the electrolysis time (h),  $V_s$  is the solution volume (L) and  $\Delta(TMP)_{exp}$  is the experimental TMP concentration decay (mg L<sup>-1</sup>).

The mineralization degree was monitored from DOC decay, measured on a Shimadzu TOC-VCSN analyzer equipped with an ASI-V auto sampler. A stoichiometric ratio of 3.7 mg L<sup>-1</sup> Na<sub>2</sub>SO<sub>3</sub> to 1 mg L<sup>-1</sup> H<sub>2</sub>O<sub>2</sub> [36] was added to the sample to quench remaining H<sub>2</sub>O<sub>2</sub> and stop the mineralization process. Total dissolved nitrogen was measured on the same analyzer coupled with a TNM-1 unit. From these data, the mineralization current efficiency (MCE, in %) was calculated by Eq. (11) [37]:

$$MCE = \frac{nF V_s \Delta(DOC)_{exp}}{4.32 \times 10^7 m I t} \times 100 \quad (11)$$

where  $F$  is the Faraday constant (96,487 C/mol),  $\Delta(DOC)_{exp}$  is the experimental DOC abatement (mg L<sup>-1</sup>),  $4.32 \times 10^7$  is a conversion factor ( $3600 \text{ s h}^{-1} \times 12,000 \text{ mg mol}^{-1}$ ) and  $m$  is the number of carbon atoms of TMP (14 carbon atoms). The  $n$ -value was taken equal to 72 assuming that TMP is mineralized to CO<sub>2</sub> with release of NH<sub>4</sub><sup>+</sup> and NO<sub>3</sub><sup>-</sup> ions, as will be discussed below, from Eq. (12):



The H<sub>2</sub>O<sub>2</sub> concentration was determined by the colorimetric metavanadate method [38]. Fe<sup>2+</sup>, Fe<sup>3+</sup> and total dissolved iron concentration were obtained according to the colorimetric 1,10-phenantroline standardized procedure [39]. UV-vis measurements were made with a VWR UV-6300PC spectrophotometer. The UVA lamp spectral irradiance was collected between 350 and 700 nm using a spectro-radiometer consisting of a mini spectrophotometer (USB2000 + UV-Vis, OceanOptics, USA) connected to an optical fiber (QP600-1-SR, OceanOptics, USA) with an irradiance probe on its tip (CC-3-UV-S cosine-corrected irradiance probe, OceanOptics, USA).

### 3. Results and discussion

#### 3.1. Characteristics of the TMP solution

A 20.0 mg L<sup>-1</sup> TMP initial concentration (DOC = 11.6 mg L<sup>-1</sup>) was used to achieve comprehensive TMP and DOC decay profiles, along with a good identification of intermediates formed.

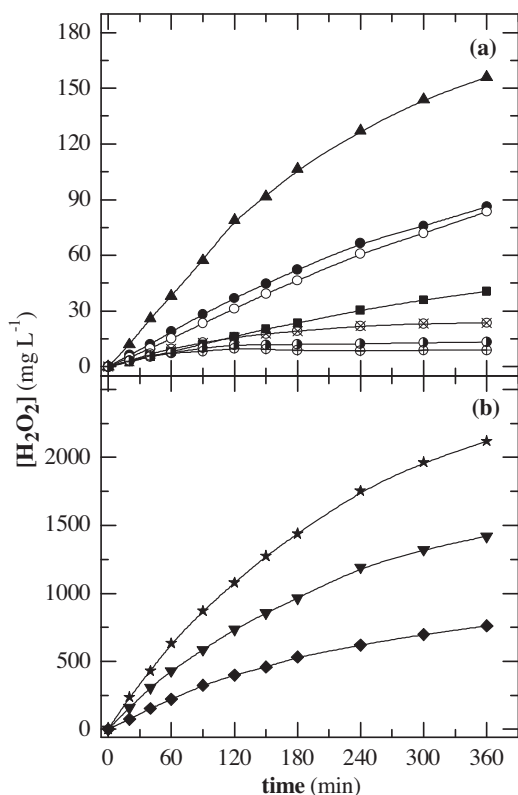
The UV-vis spectrum of TMP (Fig. 2) revealed that it absorbs radiation until ca. 310 nm with  $\lambda_{max} = 270$  nm. As a result, the drug cannot absorb the radiation of the UVA lamp and only a small fraction of the solar radiation can be absorbed (see spectral irradiance of these light sources in Fig. 2). This corroborates the negligible TMP degradation found by us after 360 min of direct photolysis under UVA and solar radiation, alone or in combination with 103 mg L<sup>-1</sup> H<sub>2</sub>O<sub>2</sub> (stoichiometric amount necessary to completely mineralize the 20.0 mg L<sup>-1</sup> TMP solution). Sirtori et al. [30] have reported that TMP was highly stable to direct photolysis under simulated sunlight during 700 min and, afterwards, it dropped rapidly up to disappear at 1100 min. This severe drop on drug content was attributed to the formation of a photoreactive intermediate, a ketone derivative (2,4-diaminopyrimidin-5-yl)(3,4,5-trimethoxyphenyl)methanone), previously reported as a potential photosensitizer of its degradation [40]. This compound was also determined in the present study, as will be discussed below.

Fig. 2 also shows that the presence of 2.0 mg L<sup>-1</sup> Fe<sup>2+</sup> did not changed the TMP absorption spectrum. In contrast, a small increment of absorbance can be observed when 2.0 mg L<sup>-1</sup> Fe<sup>3+</sup> were added, which can be ascribed to the formation Fe(III)-hydroxy complexes (see Fe<sup>3+</sup> speciation diagrams vs. pH in Fig. SM-1 of Supplementary Material). Similar spectrums were achieved for 2.0 mg L<sup>-1</sup> Fe<sup>3+</sup> solutions in the presence and absence of 7.0 g L<sup>-1</sup> Na<sub>2</sub>SO<sub>4</sub>, indicating that the formation of Fe(III)-sulfate complexes, like FeSO<sub>4</sub><sup>+</sup> and Fe(SO<sub>4</sub>)<sub>2</sub><sup>-</sup>, showed a negligible influence on the absorption spectrum at pH 3.5.

#### 3.2. Actinometric experiments

The ferrioxalate actinometry, both with crystals of K<sub>3</sub>[Fe(C<sub>2</sub>O<sub>4</sub>)<sub>3</sub>]·3H<sub>2</sub>O and [Fe(C<sub>2</sub>O<sub>4</sub>)<sub>3</sub>]<sup>3-</sup> ion prepared in situ, led to a similar photonic flux of  $1.05 \pm 0.06 \text{ J s}^{-1}$  entering the system in PEF experiments using the UVA lamp. In turn, the actinometry based on 2-NB concentration reached a smaller





**Fig. 3.** Variation of accumulated  $\text{H}_2\text{O}_2$  concentration with time during the electrolysis of 1250 mL of a  $7.0 \text{ g L}^{-1}$   $\text{Na}_2\text{SO}_4$  solution at pH 3.0 and  $20^\circ\text{C}$  in the lab-scale flow plant equipped with a  $10 \text{ cm}^2$  boron-doped diamond (BDD) anode and a  $10 \text{ cm}^2$  carbon-PTFE air-diffusion cathode at flow rate of  $40 \text{ L h}^{-1}$ . Current density: (a) (■)  $2.5$ , (●)  $5$  and (▲)  $10 \text{ mA cm}^{-2}$  and (b) (◆)  $50$ , (▼)  $100$  and (★)  $150 \text{ mA cm}^{-2}$ . Plot (a) also presents the change of  $\text{H}_2\text{O}_2$  concentration under (⊗) EF-BDD, (⊙) PEF-BDD and (⊕) SPEF-BDD conditions with  $[\text{Fe}^{2+}]_0 = 2.0 \text{ mg L}^{-1}$  at  $5 \text{ mA cm}^{-2}$  and (○) using a  $10 \text{ cm}^2$  Pt anode instead of BDD.

value of  $0.65 \pm 0.04 \text{ J s}^{-1}$ . The 2-NB actinometry implicates a more reliable experimental procedure than the above method since the associated error of samples dilution is lower and the 2-NB concentration is more stable and accurate to assess than the  $\text{Fe}^{2+}$  concentration. Hence, a photonic flux value of  $0.65 \pm 0.04 \text{ J s}^{-1}$  was applied in PEF experiments to calculate the accumulated UV energy ( $Q_{UV,n}$ ,  $\text{kJ L}^{-1}$ ). This value conveys in an accumulation of  $1.9\text{--}2.3 \text{ kJ L}^{-1}$  per h for a solution volume of  $1000\text{--}1250 \text{ mL}$  as used in our experiments.

### 3.3. $\text{H}_2\text{O}_2$ accumulation

Fig. 3a and b shows a gradual rise in  $\text{H}_2\text{O}_2$  concentration with electrolysis time for all  $j$ , giving increasing accumulations of 41, 86, 156, 760, 1420 and  $2121 \text{ mg L}^{-1}$  of this species for 2.5, 5, 10, 50, 100 and  $150 \text{ mA cm}^{-2}$ , respectively, after 360 min of electrolysis using the BDD/air-diffusion cell at flow rate of  $40 \text{ L h}^{-1}$ . This indicates a practically linear relation between accumulated  $\text{H}_2\text{O}_2$  and  $j$  due to the concomitant acceleration of its electrogeneration and decomposition reactions, Eqs. (1) and (2), respectively. At the beginning of electrolysis, the  $\text{H}_2\text{O}_2$ -time plots were practically linear, but for times longer than 180–240 min a gradual deceleration of  $\text{H}_2\text{O}_2$  accumulation was always observed, suggesting that the reaction rate of its decomposition became similar to that of its electrogeneration. Fig. 3a also highlights the effect of  $\text{Fe}^{2+}$  addition (EF-BDD conditions) along with UVA irradiation (PEF-BDD conditions) and solar irradiation (SPEF-BDD conditions) on  $\text{H}_2\text{O}_2$  accumulation at  $5 \text{ mA cm}^{-2}$ . As can be seen, under EF-BDD conditions less  $\text{H}_2\text{O}_2$  was accumulated because of its additional destruction via Fenton's

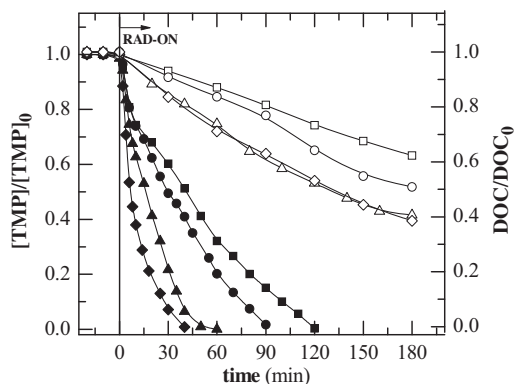


**Fig. 4.** Effect of initial  $\text{Fe}^{2+}$  concentration on (solid symbols) normalized TMP concentration decay and (open symbols) normalized DOC removal as a function of time for the PEF-BDD degradation of a  $20.0 \text{ mg L}^{-1}$  TMP solution in  $7.0 \text{ g L}^{-1}$   $\text{Na}_2\text{SO}_4$  at pH 3.0,  $10 \text{ mA cm}^{-2}$ ,  $20^\circ\text{C}$  and flow rate of  $40 \text{ L h}^{-1}$ .  $[\text{Fe}^{2+}]_0$ : (■, □)  $2.0$ , (●, ○)  $3.0$ , (▲, △)  $4.0$  and (◆, ◇)  $8.0 \text{ mg L}^{-1}$ .

reaction (5). The loss of  $\text{H}_2\text{O}_2$  was more significant in PEF-BDD conditions due to the quicker  $\text{Fe}^{2+}$  regeneration from Eq. (6), being even more pronounced under SPEF-BDD conditions since sunlight provided a greater UV intensity than the UVA light used in PEF-BDD. In addition, Fig. 3a reveals that both BDD/air-diffusion and Pt/air-diffusion cells yielded similar ability to accumulate  $\text{H}_2\text{O}_2$  at  $5 \text{ mA cm}^{-2}$ .

### 3.4. Effect of experimental parameters on the PEF process with a BDD anode

#### 3.4.1. Initial $\text{Fe}^{2+}$ concentration

A first approach to the treatment of the TMP solution was performed by varying the initial  $\text{Fe}^{2+}$  concentration from  $2.0$  to  $8.0 \text{ mg L}^{-1}$  at pH 3.0 and  $20^\circ\text{C}$  by PEF-BDD at  $10 \text{ mA cm}^{-2}$ . This pH was chosen since it has been found as optimal for a vast number of aromatics degraded by photo-Fenton, solar photo-Fenton, PEF and SPEF because the dominant iron species in solution is  $\text{FeOH}^{2+}$ , the most photoactive  $\text{Fe(III)}$ -hydroxy complex, and precipitation does not take place yet [26,40–44]. Fig. 4 depicts a progressively faster TMP concentration decay at higher initial  $\text{Fe}^{2+}$  concentration, with total removal after shorter times of 120, 90, 60 and 40 min for increasing  $\text{Fe}^{2+}$  contents of  $2.0$ ,  $3.0$ ,  $4.0$  and  $8.0 \text{ mg L}^{-1}$ , respectively. A pseudo-first-order kinetic model was fitted to the experimental data according to the procedure described in Supplementary Material. The pseudo-first-order kinetic parameters both for TMP and DOC decays are displayed in Tables SM-2 and SM-3 of Supplementary Material, respectively. Table SM-2 shows that the  $k_{\text{TMP}}$  values were 1.2, 2.3 and 4.9 times superior for  $3.0$ ,  $4.0$  and  $8.0 \text{ mg L}^{-1}$  compared with  $2.0 \text{ mg L}^{-1}$ , respectively. This trend can be related to the increasing amount of  $\text{Fe}^{2+}$  initially available and regenerated from: (i) photolysis of  $\text{FeOH}^{2+}$  through Eq. (6) and (ii) cathodic reduction of  $\text{Fe}^{3+}$  from Eq. (8), which improves the  $\cdot\text{OH}$  production from Fenton's reaction (5). In contrast, Fig. 4 reveals the existence of a poor DOC abatement in the above trials, not higher than 61% after 180 min of electrolysis, with similar removal rate for initial  $\text{Fe}^{2+}$  doses higher than  $4.0 \text{ mg L}^{-1}$ . Moreover, slightly lower  $\text{H}_2\text{O}_2$  accumulations were found for higher initial  $\text{Fe}^{2+}$  concentrations because of the existence of more  $\text{Fe}^{2+}$  available to react with  $\text{H}_2\text{O}_2$  by Fenton's reaction (5), whereas total dissolved iron concentration remained constant and equal to the initial value during all the electrolysis time (data not displayed).

Sirtori et al. [30] and Michael et al. [32] have also reported a slow and incomplete TMP mineralization by  $\text{TiO}_2$  photocatalysis and solar photo-Fenton, respectively, and have correlated these results with the formation of very stable photo-transformation products,

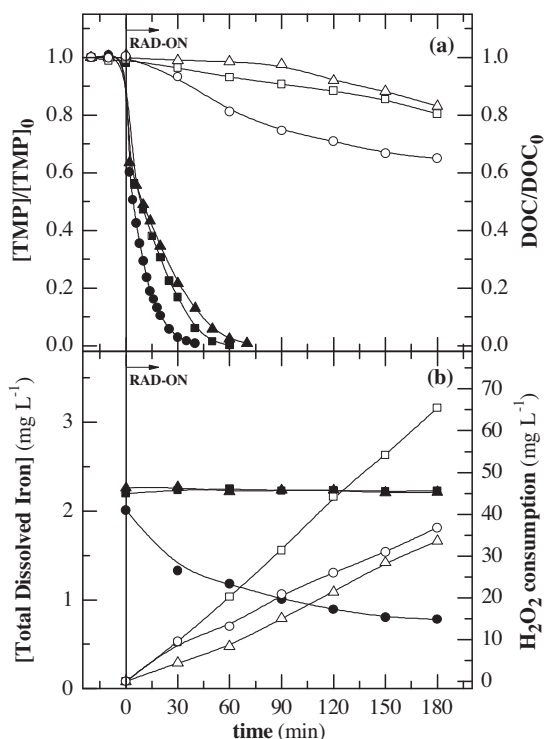


**Fig. 5.** Evaluation of the photo-Fenton process in terms of: (a) (solid symbols) normalized TMP concentration decay and (open symbols) normalized DOC removal and (b) (solid symbols) total dissolved iron concentration and (open symbols) H<sub>2</sub>O<sub>2</sub> consumption as a function of time in the flow plant for the treatment of 20.0 mg L<sup>-1</sup> TMP with [Fe<sup>2+</sup>]<sub>0</sub> = 2.0 mg L<sup>-1</sup> at pH 3.5 and 20 °C. Conditions: (■, □) 7.0 g L<sup>-1</sup> Na<sub>2</sub>SO<sub>4</sub> and total addition of stoichiometric H<sub>2</sub>O<sub>2</sub> at t = 0 min, (●, ○) absence of Na<sub>2</sub>SO<sub>4</sub> and gradual H<sub>2</sub>O<sub>2</sub> addition and (▲, △) 7.0 g L<sup>-1</sup> Na<sub>2</sub>SO<sub>4</sub> and gradual H<sub>2</sub>O<sub>2</sub> addition.

even more persistent than TMP, and the generation of carboxylic acids. These two contributions for the slow TMP mineralization will be analyzed below. Furthermore, it is well-known that the presence of sulfate and chloride ions in the medium can also inhibit the efficiency of the process [30,32,43,45,46]. In order to clarify the possible influence on TMP degradation kinetics of the high sulfate content employed in the above mentioned PEF-BDD trials (4.7 g L<sup>-1</sup> SO<sub>4</sub><sup>2-</sup> resulting from the employment of 7.0 g L<sup>-1</sup> Na<sub>2</sub>SO<sub>4</sub> as background electrolyte), two photo-Fenton trials were performed in the presence and absence of sulfate using 2.0 mg L<sup>-1</sup> Fe<sup>2+</sup> and pH 3.5. Fig. 5a shows that both TMP and DOC removals for the photo-Fenton trials were faster in the absence of sulfate ion, leading to *k*<sub>TMP</sub> and *k*<sub>DOC</sub> values 1.6 and 2.6 times superior, respectively, as can be seen in Tables SM-2 and SM-3, respectively. The lower efficiency of TMP degradation process in the presence of sulfate ions can be ascribed to four main causes: (i) the formation of complexes of sulfate with Fe<sup>3+</sup> (FeSO<sub>4</sub><sup>+</sup> and Fe(SO<sub>4</sub>)<sub>2</sub><sup>-</sup>), thereby affecting the distribution and reactivity of the iron species since the establishment of these complexes competes with the creation of much more photoactive Fe(III)-hydroxy complexes, yielding smaller amounts of FeOH<sup>2+</sup> and thus decreasing the regeneration of Fe<sup>2+</sup> and •OH production [44,45,47] (see Fe<sup>3+</sup> speciation diagrams in presence and absence of Na<sub>2</sub>SO<sub>4</sub> in Fig. SM-1); (ii) the scavenging of •OH by hydrogensulfate ion (2.1 mM at pH 3.0 as predicted by the SO<sub>4</sub><sup>2-</sup> speciation diagram) along with the formation of the weaker oxidant sulfate radical (SO<sub>4</sub><sup>•-</sup>) when compared with •OH via Eq. (15) [48] (rate constants for reactions in aqueous solution are usually within the range of 10<sup>6</sup>–10<sup>9</sup> M<sup>-1</sup> s<sup>-1</sup> for SO<sub>4</sub><sup>•-</sup> and 10<sup>7</sup>–10<sup>10</sup> M<sup>-1</sup> s<sup>-1</sup> for •OH [35,45,48]); (iii) the decomposition of H<sub>2</sub>O<sub>2</sub> through reaction with SO<sub>4</sub><sup>•-</sup> by Eqs. (16) and (17) [48]; and (iv) the oxidation reactions involving SO<sub>4</sub><sup>•-</sup> [45]. In addition, sulfate ions are considered a physical quencher of the ketone triplet state thereby leading to

degradation mechanisms diverging from those taking place in the absence of sulfate [49].

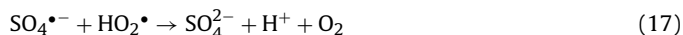
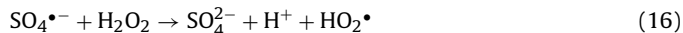
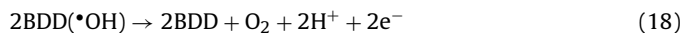


Fig. 5b depicts a gradual removal of iron from the solution up to reach around 0.8 mg L<sup>-1</sup> in the absence of sulfate ion since the introduction of this ion allows to work at higher pH values without iron precipitation as Fe(OH)<sub>3(s)</sub>. Similar amounts of H<sub>2</sub>O<sub>2</sub> were consumed in the presence and absence of sulfate (Fig. 5b). Note that the presence of Fe<sup>2+</sup> ion was omitted in the above considerations over the photo-Fenton processes since it was rapidly converted into Fe<sup>3+</sup> via Fenton's reaction (5).

Despite of the aforementioned results, an initial Fe<sup>2+</sup> content of 2.0 mg L<sup>-1</sup> was employed in the further PEF-BDD trials because: (i) the Portuguese legislation imposes this value as emission limit for the discharge of treated effluents, thus avoiding the removal of iron as a final step of the process; (ii) total iron values of 1.4–1.6 mg L<sup>-1</sup> have been found in municipal WWTPs effluents after biological treatment and so there is no need of iron addition to oxidize organics in these effluents [50,51]; and (iii) lower iron concentrations allows working at slightly higher pH values without Fe(OH)<sub>3(s)</sub> precipitation. For example, Fe<sup>3+</sup> speciation diagrams allow predicting that Fe(OH)<sub>3(s)</sub> precipitates at increasing pH values of 3.2, 3.4, 3.4 and 3.5 for declining Fe<sup>2+</sup> doses of 8.0, 4.0, 3.0 and 2.0 mg L<sup>-1</sup>, respectively.

### 3.4.2. Current density

The current density is a key parameter in the EAOPs since it regulates the amounts of oxidizing species produced. The influence of this parameter on the PEF-BDD process for TMP solution degradation was tested with 2.0 mg L<sup>-1</sup> Fe<sup>2+</sup> and pH 3.0 between 2.5 and 150 mA cm<sup>-2</sup> at 20 °C. Fig. 6a shows a gradual enhancement of TMP concentration decay when *j* increased, excluding the values between 5 and 50 mA cm<sup>-2</sup> which exhibited similar behavior. As can be seen in Table SM-2, the *k*<sub>TMP</sub> value for 2.5 mA cm<sup>-2</sup> increased up to 1.1–1.2, 1.9 and 4.1 times for 5–50, 100 and 150 mA cm<sup>-2</sup>, respectively. These findings indicate that for *j* higher than 50 mA cm<sup>-2</sup> the production of BDD(•OH) and •OH in the bulk is already large enough to rapidly degrade TMP. Nevertheless, the rise in *j* yielded higher energy consumption to destroy the drug, more apparently for values higher than 10 mA cm<sup>-2</sup> (Fig. 6b). Similarly, the DOC abatement rose when greater *j* was applied, but it was always inferior to 48% at the end of the process (Fig. 6c), suggesting the formation of by-products that are hardly oxidized by BDD(•OH), •OH and/or photodecomposed by UVA light. Since almost constant MCE values with time can be observed in Fig. 6d for each applied *j*, one can infer that the by-products formed are mineralized at similar rate during all the PEF-BDD process. Moreover, lower MCE values were achieved for raising *j* from 2.5 to 50 mA cm<sup>-2</sup>, being nearly equal between 50 and 150 mA cm<sup>-2</sup>. This loss in current efficiency with raising *j* can be related to the formation of smaller relative amounts of oxidants BDD(•OH) and •OH because of the concomitant acceleration of their waste reactions, involving, for example, the anodic oxidation of BDD(•OH) to O<sub>2</sub> via Eq. (18), the dimerization of •OH in the bulk to H<sub>2</sub>O<sub>2</sub> by Eq. (19) and the destruction of this radical with H<sub>2</sub>O<sub>2</sub> and Fe<sup>2+</sup> from Eqs. (20) and (21), respectively [22,52].



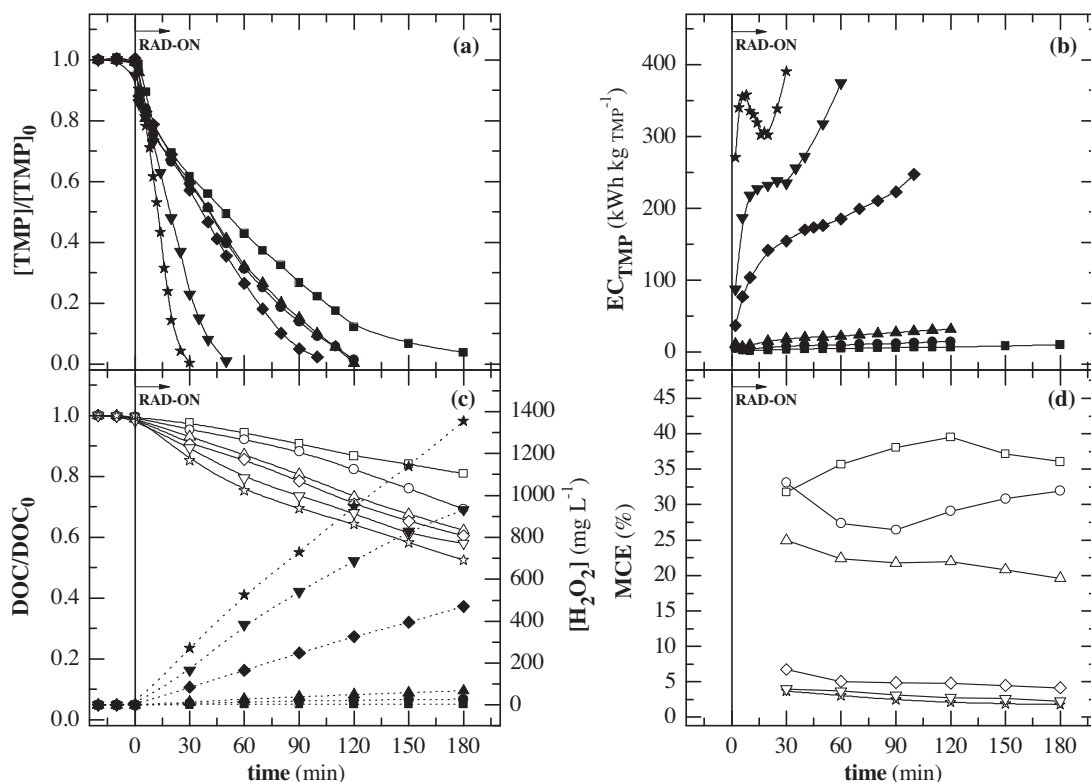


**Fig. 6.** Effect of current density on (a) normalized TMP concentration decay, (b) energy consumption per unit TMP mass, (c) (open symbols) normalized DOC removal and (dot profile)  $\text{H}_2\text{O}_2$  concentration and (d) mineralization current efficiency as a function of time for the PEF-BDD degradation of a 20.0 mg L<sup>-1</sup> TMP solution in 7.0 g L<sup>-1</sup> Na<sub>2</sub>SO<sub>4</sub> with  $[\text{Fe}^{2+}]_0 = 2.0 \text{ mg L}^{-1}$  at pH 3.0, 20 °C and flow rate of 40 L h<sup>-1</sup>. Current density: (■, □) 2.5, (●, ○) 5, (▲, △) 10, (◆, ◇) 50, (▼, ▽) 100 and (★, ☆) 150 mA cm<sup>-2</sup>.



On the other hand, Fig. 6c shows that for  $j$  of 2.5 mA cm<sup>-2</sup>,  $\text{H}_2\text{O}_2$  was consumed at the same time it was produced. In contrast, the other higher  $j$  values led to the formation in excess of  $\text{H}_2\text{O}_2$  from Eq. (1), which was accumulated during the process, thus ensuring that the system maintained the maximum production of  $\bullet\text{OH}$  from Fenton's reaction (5).

From all the above findings, a  $j$  value of 5 mA cm<sup>-2</sup> was taken for further trials because: (i) TMP concentration decay was almost similar to that obtained using 10 and 50 mA cm<sup>-2</sup>; (ii) DOC decay was within the values obtained for all the applied  $j$  but with high MCE; and (iii) the production of  $\bullet\text{OH}$  in the bulk was maximal since  $\text{H}_2\text{O}_2$  was generated in excess.

### 3.4.3. pH

The effectiveness of the PEF-BDD process was also evaluated at pH values of 3.0, 3.5, 4.0 and 4.5 using 2.0 mg L<sup>-1</sup>  $\text{Fe}^{2+}$ , 5 mA cm<sup>-2</sup> and 20 °C. The solutions with initial pH higher than 3.0 underwent a slight acidification during electrolysis and consequently their pH was continuously adjusted to the initial value by adding small volumes of 0.5 M NaOH. Although pH 3.0 has been reported as optimal for many PEF and SPEF processes [26,41,42], Fig. 7a reveals that pH values of 3.5 and 4.0 achieved similar and slightly faster TMP concentration decay. The corresponding  $k_{\text{TMP}}$  values (Table SM-2) were 1.2 and 1.1 times higher than the one reached at pH 3.0, respectively, even with an iron precipitation to values ranging from 0.76 to 1.2 mg L<sup>-1</sup> during all the pH 4.0 experiment (Fig. 7b), as predicted by Fig. SM-1b of Supplementary Material. According to this diagram, lower molar fractions of  $\text{FeOH}^{2+}$  and higher molar fractions of  $\text{FeSO}_4^+$  and  $\text{Fe}(\text{SO}_4)_2^-$  are available at pH 3.0 when compared with pH 3.5, which can justify the lower oxidizing power of PEF-BDD at pH 3.0 since Fe(III)-sulfate complexes are much less

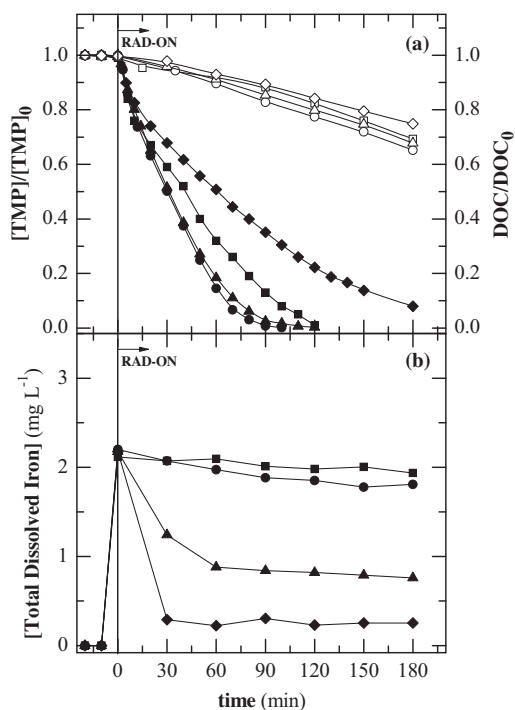


**Fig. 7.** Influence of pH on (a) (solid symbols) normalized TMP concentration decay and (open symbols) normalized DOC removal and (b) total dissolved iron concentration as a function of time for the PEF-BDD degradation of a 20.0 mg L<sup>-1</sup> TMP solution in 7.0 g L<sup>-1</sup> Na<sub>2</sub>SO<sub>4</sub> with  $[\text{Fe}^{2+}]_0 = 2.0 \text{ mg L}^{-1}$  at 5 mA cm<sup>-2</sup>, 20 °C and flow rate of 40 L h<sup>-1</sup>. Initial pH: (■, □) 3.0, (●, ○) 3.5, (▲, △) 4.0 and (◆, ◇) 4.5.

photoactive species than  $\text{FeOH}^{2+}$ , as mentioned above. Furthermore, the  $\bullet\text{OH}$  scavenging via Eq. (15) is expected to be higher at pH 3.0 than 3.5 since the  $\text{SO}_4^{2-}$  speciation diagram (data not shown) predicts hydrogensulfate amounts of 2.1 and 0.69 mM at pH 3.0 and 3.5, respectively. In turn, at pH 4.0 the  $\text{FeOH}^{2+}$  molar fraction is lower than at pH 3.0 and 3.5, but no Fe(III)-sulfate complexes are formed and no  $\bullet\text{OH}$  scavenging from Eq. (15) occurs due to the absence of hydrogensulfate ion. At pH 4.5, the slower TMP decay compared to that of pH 3.5 can be ascribed to the almost total iron precipitation (Fig. 7b). On the other hand, Fig. 7a shows a similar and very low DOC decay for all pH values tested, corresponding to removals below 31%. Taking into account the above results, a pH of 3.5 can be set as optimal for the TMP degradation under PEF-BDD conditions since it allows the fastest TMP removal without iron precipitation.

### 3.5. Comparison of AO- $\text{H}_2\text{O}_2$ , EF, PEF, SPEF, Fenton and photo-Fenton processes

The  $20.0\text{ mg L}^{-1}$  TMP solution was comparatively treated by the EAOPs tested with the BDD anode (i.e., AO- $\text{H}_2\text{O}_2$ -BDD, EF-BDD, PEF-BDD and SPEF-BDD) using the optimum conditions above established, that is,  $2.0\text{ mg L}^{-1}\text{ Fe}^{2+}$ ,  $j$  of  $5\text{ mA cm}^{-2}$  and pH 3.5. Fenton and photo-Fenton comparative trials were also carried out using  $2.0\text{ mg L}^{-1}\text{ Fe}^{2+}$  and the stoichiometric amount of  $\text{H}_2\text{O}_2$  needed for total antibiotic mineralization ( $103\text{ mg L}^{-1}$ ). Results obtained are depicted in Fig. 8. Total dissolved iron concentration remained almost constant and equal to  $2.0\text{ mg L}^{-1}$  for EF-BDD, PEF-BDD, SPEF-BDD, Fenton and photo-Fenton processes (data not displayed).

The relative power of EAOPs to degrade the TMP solution increased in the sequence AO- $\text{H}_2\text{O}_2$ -BDD < EF-BDD < PEF-BDD < SPEF-BDD (see Fig. 8a), with relative  $k_{\text{TMP}}$  values of 1:3.3:8.3:17.2 (see Table SM-2). The poorer TMP removal by AO- $\text{H}_2\text{O}_2$ -BDD can be related to the low reaction rate of TMP with the main oxidant BDD( $\bullet\text{OH}$ ) generated according to Eq. (4). In EF-BDD, the high reaction rate between the drug and  $\bullet\text{OH}$  generated from Fenton's reaction (5) improved its degradation. The faster TMP removal in PEF-BDD and SPEF-BDD evidences the additional  $\bullet\text{OH}$  production induced by the UV photolysis of photoactive  $\text{FeOH}^{2+}$  as indicated by Eq. (6). The higher UV intensity from sunlight yielded a greater rate for the latter reaction, thus explaining that SPEF-BDD is the most powerful EAOP. Note that the reaction kinetics of Fenton's based processes are influenced by temperature due to the occurrence of thermal reactions [12], whereas no effect of temperature on AO- $\text{H}_2\text{O}_2$ -BDD process is known.

Fig. 8b reveals again the superiority of DOC removal by SPEF-BDD and, in turn, PEF-BDD exhibited dominance over AO- $\text{H}_2\text{O}_2$ -BDD and EF-BDD, as can also be deduced from the  $k_{\text{DOC}}$  values given in Table SM-3. While the two latter processes only led to 11–14% mineralization after 180 min reaction, DOC was reduced by 35 and 66% in PEF-BDD and SPEF-BDD, respectively. Therefore, the supplementary  $\bullet\text{OH}$  production under UV light from Eq. (6) along with the direct photolysis of  $\text{Fe}^{3+}$  complexes with some organic intermediates like generated carboxylic acids via Eq. (7), which occurred in larger extent under the powerful UV radiation provided by sunlight, revealed to play a crucial role on TMP and its intermediates degradation.

On the other hand, Fig. 8c shows that  $\text{H}_2\text{O}_2$  was accumulated in larger extent in the order: AO- $\text{H}_2\text{O}_2$ -BDD > EF-BDD > PEF-BDD > SPEF-BDD, as expected by the increasing oxidation performance of these EAOPs, as stated above. Surprisingly, the comparison of these data with those reached for EF-BDD, PEF-BDD and SPEF-BDD in the absence of the antibiotic (see Fig. 3a) reveals that  $\text{H}_2\text{O}_2$  attained higher concentrations in the presence

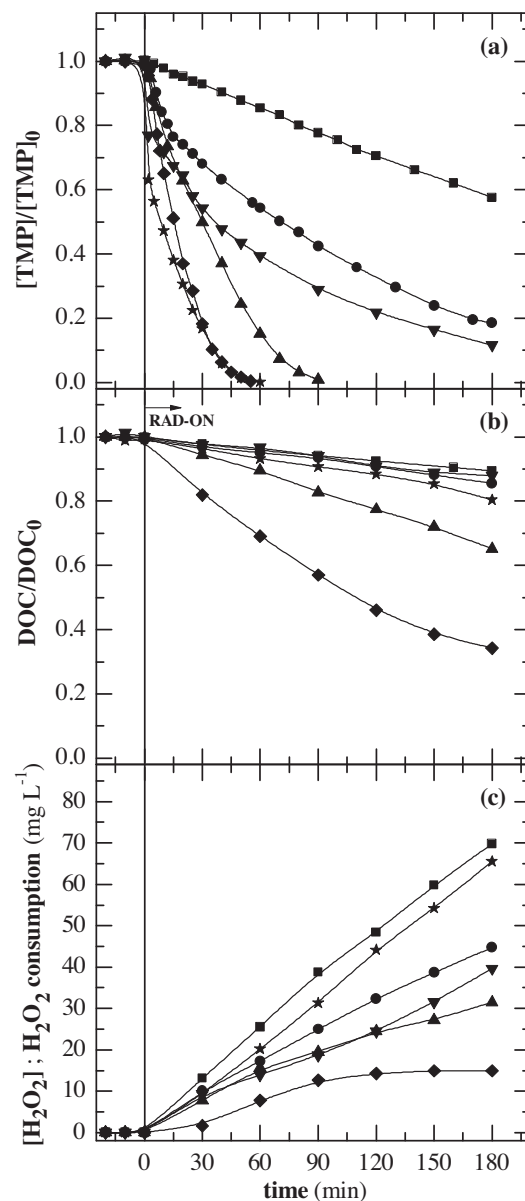


**Fig. 8.** Evaluation of (a) normalized TMP concentration decay, (b) normalized DOC removal and (c)  $\text{H}_2\text{O}_2$  concentration (for EAOPs) or  $\text{H}_2\text{O}_2$  consumption (for chemical AOPs) as a function of time for the treatment of  $20.0\text{ mg L}^{-1}$  TMP solutions in  $7.0\text{ g L}^{-1}\text{ Na}_2\text{SO}_4$  at pH 3.5,  $20^\circ\text{C}$  and flow rate of  $40\text{ L h}^{-1}$  by: (■) AO- $\text{H}_2\text{O}_2$ -BDD, (●) EF-BDD, (▲) PEF-BDD, (◆) SPEF-BDD, (▼) Fenton and (★) photo-Fenton. For the first four methods,  $5\text{ mA cm}^{-2}$  were applied, whereas for the five latter, the solution contained  $[\text{Fe}^{2+}]_0 = 2.0\text{ mg L}^{-1}$ .

of  $20.0\text{ mg L}^{-1}$  TMP (approximately the double at the end of reaction). This suggests that the oxidation of TMP and its by-products at the BDD anode competes with that of  $\text{H}_2\text{O}_2$  by Eq. (2), diminishing its decomposition rate, which means that the  $\text{H}_2\text{O}_2$  consumed during EAOPs depends on the existing pollutants and so it is complex to estimate.

Considering that EF-BDD and PEF-BDD can count on (i) BDD( $\bullet\text{OH}$ ) attack, (ii)  $\text{Fe}^{2+}$  regeneration at the cathode from Eq. (8) and (iii) even the direct oxidation of TMP on BDD in addition to the reactions occurring in the Fenton and photo-Fenton treatment, one can expect, in a simple approach, that a faster antibiotic degradation will be obtained by the EAOPs. However, there are significant differences between both chemical and electrochemical treatments for TMP degradation. In Fenton and photo-Fenton,  $\text{H}_2\text{O}_2$  is available in high concentrations at the first instant of reaction and known



amounts of this oxidant are added to the solution, allowing the calculation of the  $\text{H}_2\text{O}_2$  consumption. In contrast, in EF-BDD and PEF-BDD,  $\text{H}_2\text{O}_2$  is not present when the reaction starts and is continuously generated and consumed, depending on the presence of TMP and its intermediates, as stated formerly. Thus, when comparing these processes, the TMP and DOC decay profiles should be analyzed with precaution and no clear conclusions about efficiencies can be drawn in terms of  $\text{H}_2\text{O}_2$  consumed from TMP or DOC removed. More effective comparisons can be performed by means of (i) economic analysis; (ii) environmental impact assessment due to the fact that  $\text{H}_2\text{O}_2$  and electricity production are industrial activities that involve negative consequences to the environment; and (iii) implementation of new EF and PEF configurations that ensure  $\text{H}_2\text{O}_2$  availability from the first instant of reaction.

Fig. 8a shows that Fenton and photo-Fenton processes underwent much faster TMP decay than their electrochemical analogous during the first 2 min of reaction, where high removals of 23 and 37% were already achieved, respectively. This behavior can be related to the larger amount of  $\text{H}_2\text{O}_2$  present in solution at the start of the chemical processes with consequent maximum  $\bullet\text{OH}$  production via Fenton's reaction (5) in contrast with the lower  $\text{H}_2\text{O}_2$  concentration achieved in EF-BDD and PEF-BDD due to the  $\text{H}_2\text{O}_2$  gradual generation along time (see Fig. 8c). In order to confirm this postulation, a PEF-BDD trial with initial addition of the stoichiometric amount of  $\text{H}_2\text{O}_2$  was performed and an identical initial TMP decay of 38% after 2 min was achieved, validating what was proposed. Furthermore, one can infer a slight synergistic effect for the combination of AO- $\text{H}_2\text{O}_2$ -BDD and photo-Fenton processes, mostly in terms of DOC removal, since the  $k_{\text{TMP}}$  and  $k_{\text{DOC}}$  values of the PEF-BDD with  $\text{H}_2\text{O}_2$  addition were 1.2 and 2.5 higher than that of the sum of the corresponding constants of the individual processes (see Tables SM-2 and SM-3).

After this distinct phase in Fenton and photo-Fenton processes, the TMP degradation became slower and, similarly to other processes, followed pseudo-first-order kinetics commonly correlated to the competition between initial degradation by-products and parent compound for oxidizing species and available radiation (see  $k_{\text{TMP}}$  values in Table SM-2). However, these slow reactions can also be related to the formation of strong and stable Fe(III)-TMP complexes thereby limiting the regeneration of  $\text{Fe}^{2+}$  and consequently the overall efficiency of the process. Demirezen et al. [53] described that Fe(III)-TMP complexes are characterized by two medium metal-N stretching bands and assumed that the two  $\text{NH}_2$  groups on the pyrimidine rings act as monodentate ligands of ferric ions. Tella and Obaleye [54] reported the formation of Fe(III)-TMP complexes with a Fe(III)-to-TMP molar ratio of 1:2 and a stability constant ( $\log K$ ) of 10.99 (ionic strength = 0.1 M).

As concerns DOC abatement, Fig. 8b reveals an almost negligible mineralization by the Fenton process, slightly enhanced by EF-BDD, whereas PEF-BDD displayed a clear superiority over photo-Fenton, yielding a final mineralization of 35% against 17% after 180 min, with a  $k_{\text{DOC}}$  value 2.1 times higher (see Table SM-3). This reveals that some intermediates need UVA light to be mineralized and are faster degraded under electrochemical conditions, as expected.

A photo-Fenton trial with gradual  $\text{H}_2\text{O}_2$  addition achieved TMP and DOC removals similar to those obtained when all the  $\text{H}_2\text{O}_2$  was initially added, but  $\text{H}_2\text{O}_2$  consumption was inferior in the former approach (less than  $32 \text{ mg L}^{-1}$  after 180 min) as a consequence of undesirable waste reactions as Eq. (20) when  $\text{H}_2\text{O}_2$  is available in high amounts (see Fig. 5a and b and Tables SM-2 and SM-3).

### 3.6. BDD vs. Pt anodes in PEF and SPEF processes

The influence of BDD and Pt anodes on TMP degradation was verified under PEF and SPEF conditions using  $2.0 \text{ mg L}^{-1} \text{ Fe}^{2+}$ ,  $j$  of  $5 \text{ mA cm}^{-2}$ , pH 3.5 and  $20^\circ\text{C}$ . Fig. 9a shows that PEF-BDD exhibited

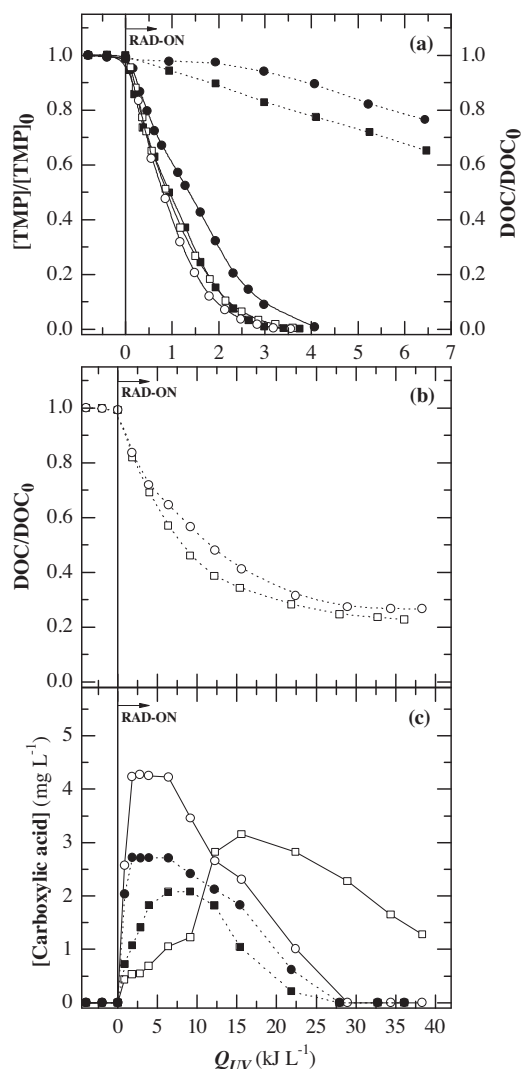


**Fig. 9.** (a and b) Influence of (■, □) BDD and (●, ○) Pt anodes on the (solid symbols) PEF and (open symbols) SPEF processes of a  $20.0 \text{ mg L}^{-1}$  TMP solution in  $7.0 \text{ g L}^{-1} \text{ Na}_2\text{SO}_4$  using  $[\text{Fe}^{2+}]_0 = 2.0 \text{ mg L}^{-1}$ , pH 3.5,  $5 \text{ mA cm}^{-2}$ ,  $20^\circ\text{C}$  and flow rate of  $40 \text{ L h}^{-1}$ . (a) (Solid profile) normalized TMP concentration decay and (dot profile) normalized DOC removal for PEF and (b) normalized DOC removal for SPEF as a function of accumulated UV energy per L of solution. In plot (c), evolution of the concentration of (■, □) oxalic and (●, ○) formic acids during (solid symbols) SPEF-BDD and (open symbols) SPEF-Pt.

slightly faster TMP and DOC removals than PEF-Pt, being its  $k_{\text{TMP}}$  and  $k_{\text{DOC}}$  values about 1.5 and 1.2 times superior, respectively (see Tables SM-2 and SM-3). In turn, SPEF-BDD and SPEF-Pt treatments yielded a less variation regarding both TMP and DOC decays (see Fig. 9a and b and Tables SM-2 and SM-3). Since it is well-known that BDD( $\bullet\text{OH}$ ) are produced in more extent than Pt( $\bullet\text{OH}$ ) from Eq. (4) [55], the minor discrepancies achieved using the both anodes confirm the minor role previously attributed to M( $\bullet\text{OH}$ ) on the degradation of TMP and its intermediates under PEF and SPEF conditions due to the strong photocatalytic action of the UV radiation, especially under the action of the sun. Furthermore, as can be seen in Fig. 9b, a quasi-steady DOC removal was achieved in SPEF-BDD and SPEF-Pt for accumulated radiations higher than ca.  $22 \text{ kJ L}^{-1}$  and incomplete DOC abatements of 73–77% were obtained after 36–38  $\text{kJ L}^{-1}$  at 420 min, thereby suggesting the formation of recalcitrant intermediates that are hardly destroyed either by BDD( $\bullet\text{OH}$ ) or Pt( $\bullet\text{OH}$ ),  $\bullet\text{OH}$  in the bulk and UV radiation provided by sunlight. The nature of these compounds will be discussed below. At the end of these trials, MCE values of 30 and 26% and energy consumptions

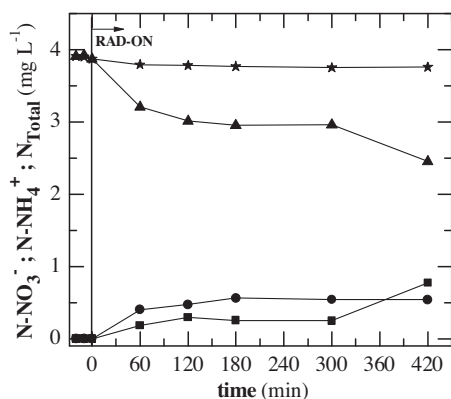


Fig. 10. Evolution of (■) nitrate ion, (●) ammonium ion, (▲) total organic nitrogen and (★) total dissolved nitrogen as a function of time during the SPEF-Pt process of Fig. 9.

of 1.2 and 0.9 kWh m<sup>-3</sup> were found for SPEF-BDD and SPEF-Pt, respectively. This brings to consider that the use of Pt coated anode is preferable for SPEF since it yields similar current efficiency with lower energy consumption than BDD one and, furthermore, this anode is much more inexpensive.

### 3.7. Evolution of generated carboxylic acids

Ion-exclusion chromatograms of electrolyzed solutions revealed the formation of final short-chain carboxylic acids such as oxalic ( $t_r$  = 8.5 min), oxamic ( $t_r$  = 11.5 min) and formic ( $t_r$  = 18.2 min) during the above SPEF-BDD and SPEF-Pt processes along 420 min. While oxalic and formic acids come from the degradation of the benzenic moieties of aromatic intermediates [16,37,56], oxamic acid is expected to be formed from the oxidation of *N*-derivatives [56,57]. All these acids are ultimate acids and thus they are directly mineralized to CO<sub>2</sub>, which can occur via reaction with M(•OH) and/or photodecarboxylation of the corresponding Fe(III)-carboxylate complexes [58,59] since in the SPEF processes the iron in solution is mainly available as Fe<sup>3+</sup>. Oxamic acid was detected in very low concentrations (<0.06 mg L<sup>-1</sup>). In contrast, oxalic and formic acid were accumulated in a larger content up to 4.3 mg L<sup>-1</sup>, as shown in Fig. 9c. While the Fe(III)-formate complexes were accumulated and removed completely at similar rate for both anodes, the Fe(III)-oxalate species were more rapidly mineralized using BDD than Pt, because they can be oxidized by BDD(•OH) but not by Pt(•OH) [16,18]. At 420 min (36–38 kJ L<sup>-1</sup>), practically no short-chain carboxylic acids were detected in both SPEF-BDD and SPEF-Pt treatments, indicating that the remaining DOC in their final solutions (23–27%) is due to the presence of other undetected and more stable by-products.

### 3.8. Nitrogen mass balance

The mineralization of TMP is expected to be accompanied by the loss of its N atoms in the form of inorganic ions such as NH<sub>4</sub><sup>+</sup>, NO<sub>3</sub><sup>-</sup> and NO<sub>2</sub><sup>-</sup>. To confirm this, the evolution of these ions was followed during the above SPEF-Pt process, where the initial solution contained 3.86 mg L<sup>-1</sup> of N. No NO<sub>2</sub><sup>-</sup> ion was detected under these conditions as expected by its instability in strong oxidant media. Fig. 10 shows the accumulation of both NH<sub>4</sub><sup>+</sup> and NO<sub>3</sub><sup>-</sup> ions up to 0.56 and 0.77 mg L<sup>-1</sup> of N at the end of electrolysis, respectively, without change in the total dissolved N concentration in solution. One can then infer that an equivalent proportion of both ions are released to the medium, as proposed in reaction

(12), and that a high amount of recalcitrant *N*-derivatives related to about 65% of total dissolved N remains in the final treated solution, which also contains 27% of the initial DOC. Similarly to these results, Sirtori et al. [30] have described the generation of low concentrations of NH<sub>4</sub><sup>+</sup> and NO<sub>3</sub><sup>-</sup> ions during the TMP degradation by TiO<sub>2</sub> photocatalysis, corresponding only to 20% of initial N, and correlated this result to the persistence of high-molecular-weight *N*-intermediates. Michael et al. [32] have also reported the presence of *N*-generated intermediates until the end of the degradation by solar photo-Fenton process of the same antibiotic.

### 3.9. Generated aromatic products

The determination of the specific ultraviolet absorbance at 254 nm (SUVA<sub>254</sub>), defined as the UV absorbance at 254 nm (in m<sup>-1</sup>) divided by the DOC concentration (in mg L<sup>-1</sup>), has been strongly correlated with the aromatic content of a solution [60]. From this measurement, the aromatic content of the TMP solution treated by the above SPEF-Pt process underwent a severe drop in its initial stages up to reach an almost constant value close to 43% of the initial SUVA<sub>254</sub> content ( $3.2 \times 10^{-4}$  L mg<sup>-1</sup> m<sup>-1</sup>). This finding in parallel with: (i) the slow TMP mineralization attained along all the treatments; (ii) the incomplete mineralization attained by SPEF processes even after the accumulation of high UV light doses; and (iii) the high residual N content, suggests the formation of high amounts of recalcitrant *N*-heteroaromatic products.

To elucidate the nature of the oxidation products, and then to check the formation of recalcitrant N products, several samples withdrawn up to 60 min of the PEF-Pt degradation of a 20.0 mg L<sup>-1</sup> TMP solution in 7.0 g L<sup>-1</sup> Na<sub>2</sub>SO<sub>4</sub> with 2.0 mg L<sup>-1</sup> Fe<sup>2+</sup> at pH 3.5, 5 mA cm<sup>-2</sup> and 20 °C, were analyzed by LC–MS. The aromatic products are mainly formed and oxidized by •OH in the bulk and a significant photocatalytic action of UV light takes place in light-induced processes, especially in SPEF due to the potent solar irradiation. Therefore, the same kind of intermediates is expected in all light-induced Fenton's reaction based AOPs/EAOPs (PEF and SPEF using Pt or BDD anode, photo-Fenton and solar photo-Fenton). Table 1 collects the 18 aromatic compounds identified, including the initial TMP (1), and 19 hydroxylated derivatives. The primary ketone product 2 has been previously described as a photoreactive intermediate causing an autocatalytic effect on TMP degradation [40]. Reactions of deamination, demethylation and/or hydroxylation of 1 lead to compounds 3–10, which maintain the two-ring TMP structure. The subsequent cleavage of 1–10 results in the benzenic derivatives 11–13 and *N*-heteroaromatics 14–18. The products 11–18 with one aromatic moiety can be more rapidly mineralized under UV radiation. The cleavage of their ring produces Fe(III)-oxamate, Fe(III)-oxalate and Fe(III)-formate complexes, which can be completely photolyzed or destroyed by BDD(•OH), as shown in Fig. 9c. It is worth mentioning that the oxidation products detected from photolysis and TiO<sub>2</sub> photocatalysis only maintained the two-ring TMP structure and major changes occurred in the trimethoxybenzyl moiety [30].

### 3.10. TMP degradation in a real wastewater matrix

To check the feasibility of degrading TMP in a realistic matrix, the most potent and cheap to run EAOP, the SPEF-Pt method, was applied under optimal conditions, i.e., 2.0 mg L<sup>-1</sup> Fe<sup>2+</sup>, 5 mA cm<sup>-2</sup>, pH 3.5 and 20 °C, to a wastewater collected after secondary treatment in an urban WWTP spiked with 20.0 mg L<sup>-1</sup> TMP. This wastewater showed: (i) neutral pH (6.8); (ii) low organic content (DOC of 12 mg L<sup>-1</sup> and chemical oxygen demand of 55 mg O<sub>2</sub> L<sup>-1</sup>); (iii) low nitrogen content (18 mg N L<sup>-1</sup>; 4.3 mg N-NH<sub>4</sub><sup>+</sup> L<sup>-1</sup>; 1.0 mg N-NO<sub>2</sub><sup>-</sup> L<sup>-1</sup>; 6.8 mg N-NO<sub>3</sub><sup>-</sup> L<sup>-1</sup>); (iv) sulfate

**Table 1**  
Aromatic products and hydroxylated derivatives from TMP degradation by PEF-Pt, identified by LC–MS both in positive and negative mode.

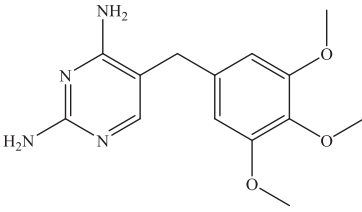
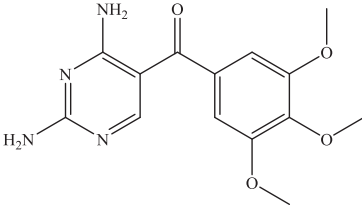
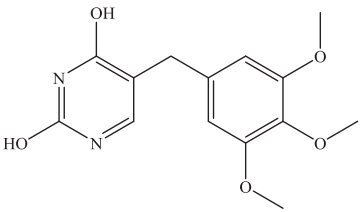
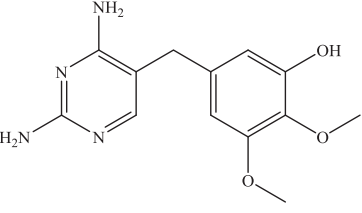
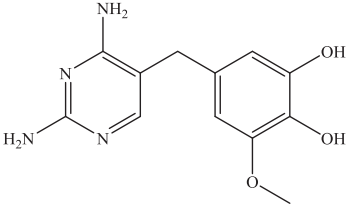
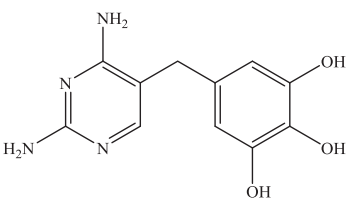
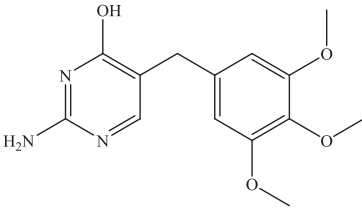
Compound	Molecular formula	Number of –OH added	<i>m/z</i>
Trimethoprim ( <b>1</b> )		–	291 <sup>a</sup>
(2,4-Diaminopyrimidin-5-yl)(3,4,5-trimethoxyphenyl)methanone ( <b>2</b> )		1 3 4	307 <sup>a</sup> 339 <sup>a</sup> 355 <sup>a</sup>
5-(3,4,5-Trimethoxybenzyl)pyrimidine-2,4-diol ( <b>3</b> )		–	–
5-((2,4-Diaminopyrimidin-5-yl)methyl)-2,3-dimethoxyphenol ( <b>4</b> )		1 3 4	305 <sup>b</sup> 337 <sup>b</sup>
5-((2,4-Diaminopyrimidin-5-yl)methyl)-3-methoxybenzene-1,2-diol ( <b>5</b> )		–	277 <sup>a</sup>
5-((2,4-Diaminopyrimidin-5-yl)methyl)-benzene-1,2,3-triol ( <b>6</b> )		1 3 4	293 <sup>a</sup> 325 <sup>a</sup> 341 <sup>a</sup>
2-Amino-5-(3,4,5-trimethoxybenzyl)pyrimidin-4-ol ( <b>7</b> )		–	–
		2 4	295 <sup>a</sup>
		–	–
		2 4	281 <sup>a</sup> 313 <sup>a</sup>
		–	289 <sup>b</sup>
		1	305 <sup>b</sup>

Table 1 (Continued)

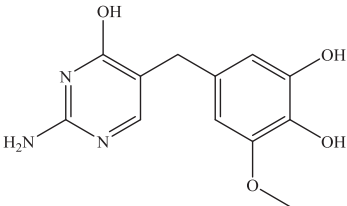
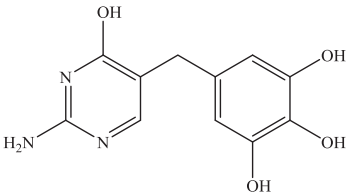
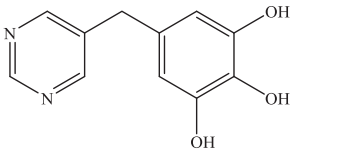
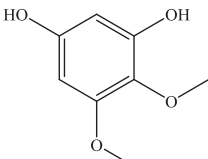
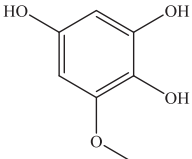
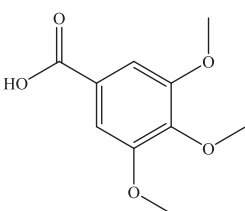
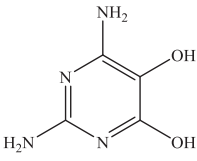
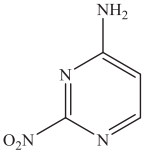
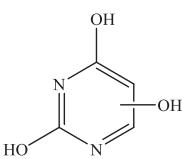
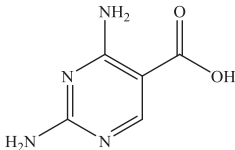
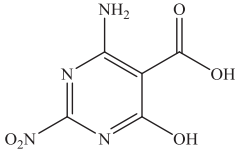
Compound	Molecular formula	Number of –OH added	m/z
		3	337 <sup>b</sup>
5-((2-Amino-4-hydroxypyrimidin-5-yl)methyl)-3-methoxybenzene-1,2-diol ( <b>8</b> )		–	261 <sup>b</sup>
5-((2-Amino-4-hydroxypyrimidin-5-yl)methyl)benzene-1,2,3-triol ( <b>9</b> )		–	247 <sup>b</sup>
5-(Pyrimidin-5-ylmethyl)benzene-1,2,3-triol ( <b>10</b> )		–	215 <sup>b</sup>
		2	247 <sup>b</sup>
		6	311 <sup>b</sup>
4,5-Dimethoxybenzene-1,3-diol ( <b>11</b> )		–	169 <sup>b</sup>
		2	201 <sup>b</sup>
6-Methoxybenzene-1,2,4-triol ( <b>12</b> )		–	–
		1	171 <sup>b</sup>
		2	187 <sup>b</sup>
3,4,5-Trimethoxybenzoic acid ( <b>13</b> )		–	211 <sup>b</sup>
		1	227 <sup>b</sup>
2,6-Diaminopyrimidine-4,5-diol ( <b>14</b> )		–	143 <sup>a</sup>
2-Nitropyrimidin-4-amine ( <b>15</b> )		–	141 <sup>a</sup>
Methanol compound with pyrimidine-2,4-diol (1:1) ( <b>16</b> )		–	127 <sup>b</sup>



Table 1 (Continued)

Compound	Molecular formula	Number of –OH added	m/z
2,4-Diaminopyrimidine-5-carboxylic acid ( <b>17</b> )		–	138 <sup>b</sup>
4-Amino-6-hydroxy-2-nitropyrimidine-5-carboxylic acid ( <b>18</b> )		–	202 <sup>a</sup>

<sup>a</sup> Positive ionization.<sup>b</sup> Negative ionization.

content of 60 mg L<sup>−1</sup>; and (v) absence of dissolved iron (see complete characterization in Table SM-1). The ionic strength of this effluent calculated on the basis of the detected ions concentrations was  $8.4 \times 10^{-3}$  M, a value ca. 18 times inferior than that of the ultrapure water with 7.0 g L<sup>−1</sup> Na<sub>2</sub>SO<sub>4</sub> matrix ( $1.48 \times 10^{-1}$  M).

No iron precipitation was disclosed by mixing the real wastewater matrix with 2.0 mg L<sup>−1</sup> Fe<sup>2+</sup> or Fe<sup>3+</sup>. However, a first SPEF-Pt trial of the 20.0 mg L<sup>−1</sup> TMP spiked effluent revealed the absence of dissolved iron after 10 min of reaction (ca. 1.0 kJ L<sup>−1</sup>), suggesting a binding of iron to the primary organic oxidation products of the wastewater. To keep an iron concentration of 2.0 mg L<sup>−1</sup> in solution along the reaction time, successive amounts of Fe<sup>2+</sup> up to 18 mg L<sup>−1</sup> were added. Nevertheless, it was observed a gradual decrease in the phosphate content from 15 mg L<sup>−1</sup> at the beginning of the process up to a final value near 1 mg L<sup>−1</sup>, indicating the probable precipitation of strengite (FePO<sub>4</sub>·2H<sub>2</sub>O).

Fig. 11 highlights the existence of slower TMP and DOC decays using the real wastewater matrix in comparison with the 7.0 g L<sup>−1</sup> Na<sub>2</sub>SO<sub>4</sub> solution, with  $k_{\text{TMP}}$  and  $k_{\text{DOC}}$  values 3.8 and 2.5 times lower, respectively (see Tables SM-2 and SM-3). After ca. 33 kJ L<sup>−1</sup> UV energy, a partial mineralization of 62 and 73% with 46 and 32% current efficiency and 1.5 and 0.8 kWh m<sup>−3</sup> energy consumption were obtained for the real wastewater and Na<sub>2</sub>SO<sub>4</sub> matrices, respectively. These results suggest the consumption of •OH, both at the anode surface and in the bulk, to oxidize the additional organic load

of the wastewater matrix, with consequent less availability of these radicals to react with TMP and its by-products. Oxalic and formic acids were found along reaction but contributing only to 1–15% of DOC content. With exception of phosphate (probable precipitation as FePO<sub>4</sub>·2H<sub>2</sub>O) and sulfate (successive addition of FeSO<sub>4</sub>·7H<sub>2</sub>O to keep dissolved iron in solution), all the other detected ions remained in their initial concentrations along the SPEF-Pt process.

#### 4. Conclusions

The degradation of a 20.0 mg L<sup>−1</sup> TMP solution in 7.0 g L<sup>−1</sup> Na<sub>2</sub>SO<sub>4</sub> could be efficiently performed in a novel 2.2 L lab-scale flow plant equipped with a BDD/air-diffusion cell by a PEF-BDD process at 20 °C using a low initial Fe<sup>2+</sup> concentration of 2.0 mg L<sup>−1</sup>, which is the Portuguese total iron discharge limit for WWTP final effluents, a current density of 5 mA cm<sup>−2</sup> and a maximum pH of 3.5 without iron precipitation. Under these conditions, H<sub>2</sub>O<sub>2</sub> was always accumulated in the medium, thus ensuring the maximum production of •OH by Fenton's reaction. The relative oxidation ability of EAOPs using the above conditions, without or with Fe<sup>2+</sup> addition, increased in the order: AO-H<sub>2</sub>O<sub>2</sub> < EF < PEF < SPEF. The slow removal of the antibiotic under AO-H<sub>2</sub>O<sub>2</sub>-BDD conditions was due to its low reaction with BDD(•OH) formed at the anode. The faster removal by EF-BDD, PEF-BDD and SPEF-BDD can be related to its high reaction rate with •OH produced in the bulk. In PEF-BDD, TMP was more rapidly degraded than in EF-BDD as a result of the additional •OH production induced by UVA irradiation. The most potent EAOP was SPEF-BDD because the more potent UV intensity supplied by sunlight led to more •OH production yielding higher TMP and DOC removals with the occurrence in larger extent of the photolysis of generated Fe(III)-carboxylate complexes. Comparison of classical Fenton and photo-Fenton processes with EF-BDD and PEF-BDD ones, respectively, demonstrated that electrochemical contributions, like BDD(•OH) attack and Fe<sup>2+</sup> regeneration from cathodic reduction of Fe<sup>3+</sup>, played an important role in the mineralization enhancement of intermediates. The TMP decay underwent a greater drop at the beginning of the chemical processes due to the higher initial availability of H<sub>2</sub>O<sub>2</sub>. The PEF process led to a slightly faster antibiotic degradation using a BDD anode instead of a Pt one, but operating in SPEF the influence of the anode was insignificant. In all the methods tested, a slow and partial TMP mineralization was found, which can be linked to two main causes: (i) the formation of a high content of hardly oxidizable N-derivatives that remained in solution up to the end of the treatment, containing the major part of N; and (ii) the presence of sulfate ion in the background electrolyte, leading to the formation of Fe(III)-sulfate

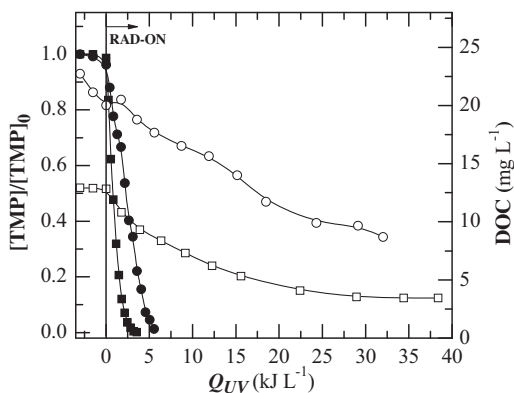


Fig. 11. (Solid symbols) Normalized TMP concentration decay and (open symbols) normalized DOC removal as a function of accumulated UV energy per L of solution for the SPEF-Pt treatment of a 20.0 mg L<sup>−1</sup> TMP solution using [Fe] = 2.0 mg L<sup>−1</sup>, pH 3.5, 5 mA cm<sup>−2</sup>, 20 °C, flow rate of 40 L h<sup>−1</sup> and two distinct matrices: (■, □) ultrapure water with 7.0 g L<sup>−1</sup> Na<sub>2</sub>SO<sub>4</sub> and (●, ○) real wastewater.

complexes instead of more potent photoactive species like  $\text{FeOH}^{2+}$  and favoring the  $\bullet\text{OH}$  scavenging to yield the less reactive  $\text{SO}_4^{\bullet-}$ . After 420 min of SPEF-BDD and SPEF-Pt consuming ca.  $37 \text{ kJ L}^{-1}$  UV energy, a partial mineralization of 77 and 73% with 30 and 26% current efficiency and 1.2 and  $0.9 \text{ kWh m}^{-3}$  energy consumption were obtained, respectively. The Pt coated anode, less expensive than the BDD one, seems then preferable to be used in SPEF. Low amounts of carboxylic acids were generated and completely removed from the solution by these methods. Up to 18 aromatic products and 19 hydroxylated derivatives were detected by LC-MS over the PEF-Pt process. TMP and DOC were slowly removed in the presence of a real wastewater matrix by SPEF-Pt, probably due to the use of  $\bullet\text{OH}$  to oxidize the additional organic content of the effluent.

## Acknowledgements

Financial support was partially provided by (i) project Pest-C/EQB/LA0020/2013, financed by FEDER through COMPETE – *Programa Operacional Factores de Competitividade*, (ii) FCT – *Fundação para a Ciência e a Tecnologia*, (iii) QREN and (iv) ON2. F.C. Moreira acknowledges her Doctoral fellowship SFRH/BD/80361/2011 supported by FCT. S. Garcia-Segura thanks the Doctoral grant awarded from MEC (Ministerio de Educación y Ciencia, Spain). V.J.P. Vilar acknowledges the FCT Investigator 2013 Programme (IF/01501/2013).

## Appendix A. Supplementary data

Supplementary data associated with this article can be found, in the online version, at <http://dx.doi.org/10.1016/j.apcatb.2014.05.052>.

## References

- [1] K. Kümmerer, *Chemosphere* 45 (2001) 957–969.
- [2] M.A. Sousa, C. Gonçalves, V.J.P. Vilar, R.A.R. Boaventura, M.F. Alpendurada, *Chem. Eng. J.* 198–199 (2012) 301–309.
- [3] K. Kümmerer, *J. Environ. Manage.* 90 (2009) 2354–2366.
- [4] M. Klavarioti, D. Mantzavinos, D. Kassinos, *Environ. Int.* 35 (2009) 402–417.
- [5] O.A.H. Jones, N. Voulvoulis, J.N. Lester, *Crit. Rev. Environ. Sci. Technol.* 35 (2005) 401–427.
- [6] M.D. Hernando, M. Mezcuá, A.R. Fernández-Alba, D. Barceló, *Talanta* 69 (2006) 334–342.
- [7] J. Burchall, in: J. Corcoran, F. Hahn, J.F. Snell, K.L. Arora (Eds.), *Mechanism of Action of Antimicrobial and Antitumor Agents*, Springer, Berlin, Heidelberg, 1975, pp. 304–320.
- [8] A.J. Watkinson, E.J. Murby, D.W. Kolpin, S.D. Costanzo, *Sci. Total Environ.* 407 (2009) 2711–2723.
- [9] B. Li, T. Zhang, *Chemosphere* 83 (2011) 1284–1289.
- [10] S. Miralles-Cuevas, A. Arqués, M.I. Maldonado, J.A. Sánchez-Pérez, S. Malato Rodríguez, *Chem. Eng. J.* 224 (2013) 89–95.
- [11] A. Pérez-González, A.M. Urtiaga, R. Ibáñez, I. Ortiz, *Water Res.* 46 (2012) 267–283.
- [12] S. Malato, P. Fernández-Ibáñez, M.I. Maldonado, J. Blanco, W. Gernjak, *Catal. Today* 147 (2009) 1–59.
- [13] S. Irmak, H.I. Yavuz, O. Erbatur, *Appl. Catal. B: Environ.* 63 (2006) 243–248.
- [14] M.A. Oturan, N. Oturan, C. Lahitte, S. Trevin, *J. Electroanal. Chem.* 507 (2001) 96–102.
- [15] C. Flox, J.A. Garrido, R.M. Rodríguez, P.L. Cabot, F. Centellas, C. Arias, E. Brillas, *Catal. Today* 129 (2007) 29–36.
- [16] M. Skoumal, R.M. Rodríguez, P.L. Cabot, F. Centellas, J.A. Garrido, C. Arias, E. Brillas, *Electrochim. Acta* 54 (2009) 2077–2085.
- [17] E. Brillas, J.A. Garrido, R.M. Rodríguez, C. Arias, P.L. Cabot, F. Centellas, *Portug. Electrochim. Acta* 26 (2008) 15–46.
- [18] E. Brillas, M.A. Baños, M. Skoumal, P.L. Cabot, J.A. Garrido, R.M. Rodríguez, *Chemosphere* 68 (2007) 199–209.
- [19] M. Hamza, R. Abdelhedi, E. Brillas, I. Sirés, *J. Electroanal. Chem.* 627 (2009) 41–50.
- [20] I. Sirés, N. Oturan, M.A. Oturan, R.M. Rodríguez, J.A. Garrido, E. Brillas, *Electrochim. Acta* 52 (2007) 5493–5503.
- [21] E. Brillas, I. Sirés, M.A. Oturan, *Chem. Rev.* 109 (2009) 6570–6631.
- [22] Y. Sun, J.J. Pignatello, *Environ. Sci. Technol.* 27 (1993) 304–310.
- [23] B.C. Faust, R.G. Zepp, *Environ. Sci. Technol.* 27 (1993) 2517–2522.
- [24] S. Garcia-Segura, E. Brillas, *Water Res.* 45 (2011) 2975–2984.
- [25] Y. Zuo, J. Hoigne, *Environ. Sci. Technol.* 26 (1992) 1014–1022.
- [26] C. Flox, P.L. Cabot, F. Centellas, J.A. Garrido, R.M. Rodríguez, C. Arias, E. Brillas, *Appl. Catal. B: Environ.* 75 (2007) 17–28.
- [27] J.-J. Aaron, M.A. Oturan, *Turk. J. Chem.* 25 (2001) 509–520.
- [28] T.A. Ternes, J. Stüber, N. Herrmann, D. McDowell, A. Ried, M. Kampmann, B. Teiser, *Water Res.* 37 (2003) 1976–1982.
- [29] M.N. Abellán, J. Giménez, S. Esplugas, *Catal. Today* 144 (2009) 131–136.
- [30] C. Sirtori, A. Agüera, W. Gernjak, S. Malato, *Water Res.* 44 (2010) 2735–2744.
- [31] I.N. Dias, B.S. Souza, J.H.O.S. Pereira, F.C. Moreira, M. Dezotti, R.A.R. Boaventura, V.J.P. Vilar, *Chem. Eng. J.* 247 (2014) 302–313.
- [32] I. Michael, E. Hapeshi, V. Osorio, S. Perez, M. Petrovic, A. Zapata, S. Malato, D. Barceló, D. Fatta-Kassinos, *Sci. Total Environ.* 430 (2012) 167–173.
- [33] T. González, J.R. Domínguez, P. Palo, J. Sánchez-Martín, E.M. Cuerda-Correa, *Desalination* 280 (2011) 197–202.
- [34] S. Malato, J. Blanco, A. Vidal, C. Richter, *Appl. Catal. B: Environ.* 37 (2002) 1–15.
- [35] G.V. Buxton, C.L. Greenstock, W.P. Helman, A.B. Ross, *J. Phys. Chem. Ref. Data* 17 (1988) 513–886.
- [36] W. Liu, S.A. Andrews, M.I. Stefan, J.R. Bolton, *Water Res.* 37 (2003) 3697–3703.
- [37] M. Skoumal, C. Arias, P.L. Cabot, F. Centellas, J.A. Garrido, R.M. Rodríguez, E. Brillas, *Chemosphere* 71 (2008) 1718–1729.
- [38] R.F.P. Nogueira, M.C. Oliveira, W.C. Paterlini, *Talanta* 66 (2005) 86–91.
- [39] ISO 6332:1988 Water Quality – Determination of iron – Spectrometric Method Using 1,10-Phenanthroline, 1998.
- [40] S. Canonica, U. Jans, K. Stemmler, J. Hoigne, *Environ. Sci. Technol.* 29 (1995) 1822–1831.
- [41] L.C. Almeida, S. Garcia-Segura, C. Arias, N. Bocchi, E. Brillas, *Chemosphere* 89 (2012) 751–758.
- [42] S. Garcia-Segura, L.C. Almeida, N. Bocchi, E. Brillas, *J. Hazard. Mater.* 194 (2011) 109–118.
- [43] J.J. Pignatello, *Environ. Sci. Technol.* 26 (1992) 944–951.
- [44] A. Safarzadeh-Amiri, J.R. Bolton, S.R. Cater, *Solar Energy* 56 (1996) 439–443.
- [45] J. De Laat, G. Truong Le, B. Legube, *Chemosphere* 55 (2004) 715–723.
- [46] M.-C. Lu, J.-N. Chen, C.-P. Chang, *Chemosphere* 35 (1997) 2285–2293.
- [47] H.-J. Benkelberg, P. Warneck, *J. Phys. Chem.* 99 (1995) 5214–5221.
- [48] P. Neta, R.E. Huie, A.B. Ross, *J. Phys. Chem. Ref. Data* 17 (1988) 1027–1247.
- [49] D. Gan, M. Jia, P.P. Vaughan, D.E. Falvey, N.V. Blough, *J. Phys. Chem. A* 112 (2008) 2803–2812.
- [50] N. De la Cruz, L. Esquiú, D. Grandjean, A. Magnet, A. Tungler, L.F. de Alencastro, C. Pulgarín, *Water Res.* 47 (2013) 5836–5845.
- [51] N. De la Cruz, J. Giménez, S. Esplugas, D. Grandjean, L.F. de Alencastro, C. Pulgarín, *Water Res.* 46 (2012) 1947–1957.
- [52] B. Marselli, J. Garcia-Gomez, P.A. Michaud, M.A. Rodrigo, C. Comninellis, *J. Electrochem. Soc.* 150 (2003) D79–D83.
- [53] N. Demirezen, D. Tarınç, D. Polat, M. Çeşme, A. Gölcü, M. Tümer, *Spectrochim. Acta A: Mol. Biomol. Spectrosc.* 94 (2012) 243–255.
- [54] A.C. Tella, J.A. Obaleye, *Int. J. Chem. Sci.* 8 (2010) 1675–1683.
- [55] A. Kapalka, G. Fóti, C. Comninellis, *J. Appl. Electrochem.* 38 (2008) 7–16.
- [56] I. Sirés, J.A. Garrido, R.M. Rodríguez, P.L. Cabot, F. Centellas, C. Arias, E. Brillas, *J. Electrochem. Soc.* 153 (2006) D1–D9.
- [57] R. Andreozzi, V. Caprio, R. Marotta, D. Vogna, *Water Res.* 37 (2003) 993–1004.
- [58] N.K. Vel Leitner, M. Doré, *Water Res.* 31 (1997) 1383–1397.
- [59] M.A. Oturan, M. Pimentel, N. Oturan, I. Sirés, *Electrochim. Acta* 54 (2008) 173–182.
- [60] J.L. Weishaar, G.R. Aiken, B.A. Bergamaschi, M.S. Fram, R. Fujii, K. Mopper, *Environ. Sci. Technol.* 37 (2003) 4702–4708.